

High Eddington quasars as discovery tools: current state and challenges

Swayamtrupta Panda^{1,†,*} and Paola Marziani²

¹*Laboratório Nacional de Astrofísica - MCTI, R. dos Estados Unidos, 154 - Nações, Itajubá - MG, 37504-364, Brazil*

²*INAF-Astronomical Observatory of Padova, Vicolo dell'Osservatorio, 5, 35122 Padova PD, Italy*

Correspondence[†]:
Swayamtrupta Panda
spanda@lna.br

ABSTRACT

A landmark of accretion processes in active galactic nuclei (AGN) is the continuum originating from a complex structure, i.e. an accretion disk and a corona around a supermassive black hole. Modelling the broad-band spectral energy distribution (SED) effectively ionizing the gas-rich broad emission line region (BLR) is key to understanding the various radiative processes at play and their importance that eventually leads to the emission from diverse physical conditions. Photoionization codes are a useful tool to investigate two aspects, the importance of the shape of the SED, and the physical conditions in the BLR. In this work, we critically review long-standing issues pertaining to the SED shape and the anisotropic continuum radiation from the central regions around the accreting supermassive black holes (few 10-100 gravitational radii), with a focus on black holes accreting at high rates, possibly much above the Eddington limit. The anisotropic emission is a direct consequence of the development of a geometrically and optically thick structure at regions very close to the black hole due to a marked increase in the accretion rates. The analysis presented in this paper took advantage of the look at the diversity of the type-1 AGN provided by the main sequence of quasars. The main sequence permitted us to assess the importance of the Eddington ratio and hence to locate the super Eddington sources in observational parameter space, as well as to constrain the distinctive physical conditions of their line-emitting BLR. This feat is posing the basis for the exploitation of quasars as cosmological distance indicators, hopefully allowing us to use the fascinating super Eddington quasars up to unprecedented distances.

Keywords: galaxies: active, quasars: emission lines; quasars: supermassive black holes; quasars: accretion, accretion disks; quasars: reverberation mapping; cosmology

1 ACTIVE GALACTIC NUCLEI AS ACCRETING BLACK HOLES

Active galactic nuclei (AGNs) are among the brightest cosmic objects known to us (Weedman, 1976, 1977). They harbour a supermassive black hole (SMBH) at their very centres which due to its immense gravitational potential allows for the infalling of matter. This in-falling matter loses angular momentum while being accreted onto the black hole. This accreted matter manifests in the form of a multi-colour

*CNPq Fellow

accretion disk which gets heated up and radiates (Shakura and Sunyaev, 1973; Shields, 1978; Czerny and Elvis, 1987; Panda et al., 2018). The photon energy of the dissipated radiation spans a wide range of energies (from sub-eV to hundreds of eVs). The emitted photons then illuminate the material surrounding the accretion disk and lead to the formation and emission of strong, broad emission lines (Schmidt, 1963; Greenstein and Schmidt, 1964; Schmidt and Green, 1983; Osterbrock and Ferland, 2006; Netzer, 2015).

2 THEIR SPECTRAL ENERGY DISTRIBUTION

AGN are observed over the entire range of the electromagnetic spectrum from the radio regime up to MeV-GeV-TeV energy γ -rays (Richards et al., 2006; Harrison, 2014; Yang et al., 2022). The classical view of AGN characterized by an almost flat spectral energy distribution (SED) over many decades in frequency – to juxtapose to the ones of non-active galaxies – has been superseded and extended since long (Malkan and Sargent, 1982; Malkan, 1983), by the recognition that the SED is different for AGN in different accretion states, and is most often characterized by significant features associated with diverse processes and aptly called bump or excess (i.e., IR excess, big blue bump, soft-X excess, etc.)^{*}

In this contribution, we shall restrict the attention mainly to the ionizing continuum in radio-quiet quasars. In this case, various components of the SED arise due to different radiation mechanisms and at varying distances, notably among them:

1. The characteristic ‘Big Blue Bump’ (Czerny and Elvis, 1987; Shields, 1978) that is formed by the optical and ultraviolet radiation produced due to thermal emission from the accretion disk.
2. The X-ray emission well-fit by a power-law, and produced when the UV photons from the disk undergo inverse Compton scattering by hot electrons in a Compton-thin corona close to the SMBH (e.g., Zdziarski et al., 1990).
3. A spectral component observationally described as a “soft X-ray excess” (e.g., Arnaud et al., 1985). The most widely-accepted interpretation of the excess detected in soft X-rays is of emission in a Compton-thick corona connected with the innermost accretion disk (Walter and Fink 1993; Petrucci et al. 2020 and references therein). The competing model – relativistically blurred photoionized disc reflection (Ross and Fabian, 2005; Crummy et al., 2006) – is not anymore favoured as an explanation for the soft X-ray excess itself, although blurred accretion disk reflection can occur independently from the soft excess (Boissay et al., 2016). The soft excess helps bridge the absorption gap between the UV downturn and the soft X-ray upturn (e.g., Elvis et al., 1994; Laor et al., 1997; Richards et al., 2006; Kubota and Done, 2018), and changes the far-UV and soft-X-ray part of the spectrum, affecting the line production, including Fe II emission in the BLR (Panda et al., 2019a).

The “intrinsic” AGN continuum at photon energies high enough to ionize Hydrogen is therefore made of the thermal emission from the accretion disk, the power-law emission from the corona, and soft X-ray excess (Collinson, 2016; Kubota and Done, 2018; Panda et al., 2019c; Ferland et al., 2020). Figure 1 shows templates for quasars believed to radiate at moderate or high Eddington ratio, $\eta \gtrsim 0.1 - 0.2$ (Population A and extreme Population A, hereafter xA, Marziani and Sulentic 2014a and §3.3.2), along with widely-exploited templates believed to be appropriate for populations of quasars radiating in this range (Mathews and Ferland, 1987; Marziani and Sulentic, 2014a; Ferland et al., 2020). There is a notable

^{*}The old description of AGN continuum as non-thermal, featureless was perhaps inspired by the earliest quasars studied that were mainly radio loud and at any rate sub-Eddington accretors. The power-law function used to fit the optical/UV continuum over a limited range in frequency is now considered to represent the thermal continuum from an accretion disk, whose power $P_\nu \propto \nu^{\frac{1}{3}}$ (Shakura and Sunyaev, 1973), not as associated with a featureless synchrotron continuum. The synchrotron radiation from relativistic jets that accounts for most of the radio emission is only a fraction of the optical continuum in non-blazar type-1 AGN or “thermal” radio-loud AGN (Antonucci, 2012, and references therein).

similarity between the curves. The SED defined by Marziani and Sulentic (2014a) for sources radiating close to the Eddington limit is in good agreement with the high case of Ferland et al. (2020). There is an increase in big blue bump prominence from the high to the highest case, the latter being associated with extreme values of the Eddington ratios. Note that the soft-X ray excess, located between the optical-UV bump and the peak at the hard X-ray (~ 100 keV), is prominent in between ~ 1 keV and 20 keV regions for the SED corresponding to the highest Eddington ratio case (magenta curve in Figure 1) and marginally present in the high case (blue curve in Figure 1). One notices that this feature steepens with $\Gamma > 2$ as the Eddington ratio increases (Jin et al., 2012b; Ferland et al., 2020). The feature almost disappears when one transitions to low Eddington ratio sources - see the blue dashed and grey SEDs, where the X-ray bump close to 100 keV is increasingly prominent.

A weak but statistically significant correlation between hard-X photon index Γ and Eddington ratio has been found (Trakhtenbrot et al., 2017; Panagiotou and Walter, 2020; Liu et al., 2021), and the statistical weaknesses might be explained by the limited range of hard Γ values compared to uncertainties in individual Γ estimates (Wang et al., 2013). In the highest case, the soft and hard X-ray domains are very steep to the point that a turnover at ~ 100 keV as seen in Figure 1 for the Mathews and Ferland (1987) SED may not be anymore required. The difference between the Mathews and Ferland (1987) SED and the extreme case of Ferland et al. (2020) exemplifies this trend. The existence of X-ray weak type-1 AGN and their high prevalence among highly accreting sources (Zappacosta et al., 2020; Laurenti et al., 2022) may also support the absence of a prominent Compton-thin coronal component in super-Eddington sources. The sequence of SEDs in Figure 1 is related to the 4DE1 parameter space (Section 3.3), although its connection to some of the parameters is still incomplete.

A related issue is the location of the high energy downturn around ~ 100 keV that is required by limits in the measured X-ray background (Mathews and Ferland, 1987). Observations are mostly available up to ~ 20 keV, and the energy of the downturn is conventionally placed at ≈ 100 keV in the SEDs of Figure 1 although it was not actually measured. In recent years measurements by NuSTAR and γ -ray observatories such as SWIFT indicate a dispersion in the actual turnover, from 50 to 200 keV (Fabian et al., 2015; Lubiński et al., 2016). It is currently debated whether the downturn energy may depend on the Eddington ratio, although the trend between Γ and the Eddington ratio suggests that a weak correlation might be possible (Ricci et al., 2018, although see Molina et al. 2019). However, we note that there are studies of multiple sources with cut-off energies measured by NuSTAR where the authors suggest that this cut-off energy is not dependent on the Eddington ratio or the black hole mass (see e.g., Tortosa et al., 2018; Kamraj et al., 2022).

The focus of Figure 1 is for $\log \epsilon [\text{Ryd}] \gtrsim -1$. We mention in passing that in the NIR domain, as the low energy tail of the AD emission fades, extrinsic emission is actually reprocessed emission from the dusty torus which surrounds the accretion disk. It becomes the dominant emission at a few μm , along with the polar dust in the direction of SMBH spin axis (Netzer, 2015; Padovani et al., 2017). In the FIR, the SED might be dominated by dust heated by host galaxy star formation, more than by the AGN itself (Kirkpatrick et al., 2015). This is occurring in systems with high accretion rate (e.g., Marziani et al., 2021b). In the case of highly accreting quasars, there is a relatively large prevalence of sources with high radio power, with radio-to-optical ratio $\gtrsim 1$ (Ganci et al., 2019; Wang et al., 2022), whose radio emission can be ascribed to star formation processes. Highly-accreting quasars might be predominantly seen as young or rejuvenated active nuclei whose SED is affected by star formation processes (see e.g., Caccianiga et al., 2015; Ganci et al., 2019).

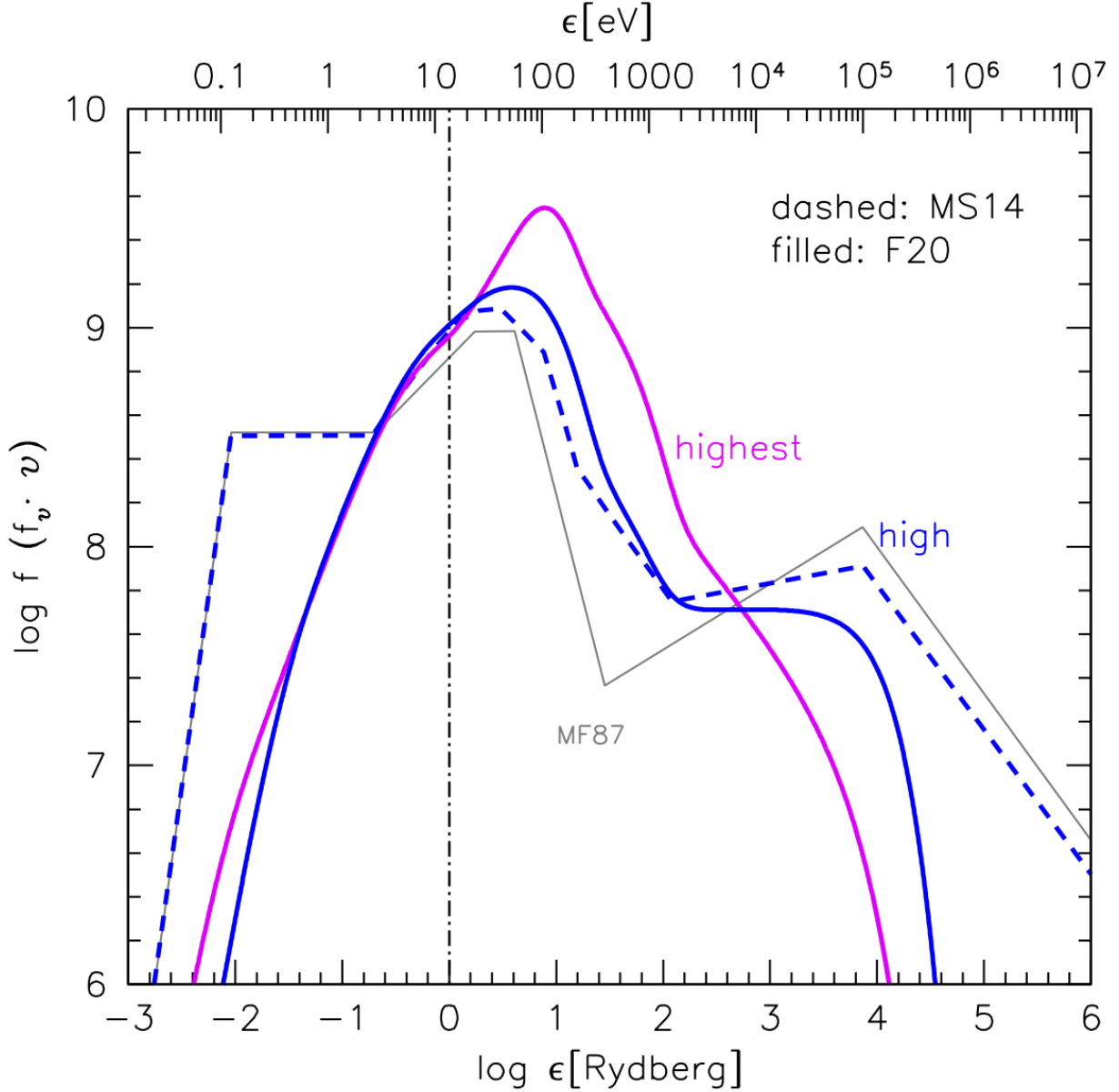


Figure 1. Templates of SEDs for high Eddington radiators. Grey; the landmark Mathews and Ferland (1987) SED; dashed blue: the Marziani and Sulentic (2014a) SED for quasars radiating close to the Eddington limit; blue and magenta: high and highest Eddington ratio templates from Ferland et al. (2020)). The SEDs have been normalized at $\epsilon \approx 0.18$ Ryd.

3 IMMINENT CHALLENGES AND OPPORTUNITIES

3.1 What an AGN multi-frequency spectrum can reveal to us?

From an observer's point of view, we can largely quantify the spectrum into two primary components: (1) the emission lines originating from the BLR/NLR clouds; and (2) the AGN continuum, prominent beyond the Lyman limit, that can photoionize the surrounding gas leading to line emission. The ionizing photon flux can be estimated by a careful analysis of the AGN SED, which then gives us a rough idea of the expected line fluxes for the multitude of ionic species (in their various ionization states) that we see in an AGN spectrum. A careful assessment of the density of these ionized clouds and their locations, in addition to the incident photon flux received by them, allows us to *predict* the strengths of these lines. Important

information about density, ionization conditions, and dynamics in the broad line-emitting region of AGN can be inferred from UV spectroscopic observations which are crucial to understanding these line-emitting regions. Past studies of highly-accreting quasars have *in turn* illustrated the use of certain line diagnostic ratios from observed spectra (e.g., C IV/He II, AlIII λ 1860/SiIII λ 1892, Fe II/H β) in order to estimate these (density, ionization condition, and metallicity) parameters (Negrete et al., 2012, 2014; Śniegowska et al., 2021; Garnica et al., 2022, and references therein). Curiously, these extreme sources appear to be characterized by values of density, ionization, and metallicity that are extreme but also extremely well-defined: as far as the virialized emitting region is concerned the parameters reach $n_{\text{H}} \sim 10^{13} \text{ cm}^{-3}$, $\log U \sim -2.5$, $Z \gtrsim 20Z_{\odot}$.[†]

3.2 Dichotomy in optical and UV emission line profiles

Historically, the BLR clouds were modelled as single clouds where the different lines arise from different parts of the same cloud - a picture that is still widely accepted (Kwan and Krolik, 1981, see the BLR radial structure as shown by Negrete et al. 2012). In the mid-1980s, propositions were made to explain the BLR as two distinct components (Collin-Souffrin et al., 1988; Gaskell, 1982). The broad emission spectrum in AGNs can be divided into two parts: the first set of lines that include Ly α , C III], C IV, He I, He II, and N V predominantly emitted by a highly ionized region that presumably has a relatively low density ($\lesssim 10^{10} \text{ cm}^{-3}$). These are known as High Ionization Lines (HILs). The upper limit to the density of the media emitting these HILs is set by the semi-forbidden CIII] in order not to be collisionally de-excited even if the actual measurement of the blueshifted C III] is problematic because of the blending with SiIII] λ 1892. As a matter of fact, the density of the outflow is poorly constrained, and there is good reason to believe that a “clumpy” scenario (e.g., Takeuchi et al., 2013) might be also appropriate. The second set of lines includes the bulk of the Balmer lines, Mg II, Fe II, O I and Ca II, emitted by a mildly ionized medium having a much higher density ($\gtrsim 10^{10} \text{ cm}^{-3}$). The real scenario is more convoluted and the search for a global unified picture is still ongoing. However, this representation — dichotomy into LILs and HILs originating from the vicinity of the SMBH due to the inherent radiation of the accretion disk — has been instrumental to identify a low-ionization virialized component and the contribution of a high ionization wind (Leighly, 2004; Marziani et al., 2010), that proved to be especially prominent in highly accreting sources i.e., quasar radiating at maximum radiative output per unit mass (Martínez-Aldama et al., 2019; Panda, 2022). Low-ionization lines retain fairly symmetric profiles that indicate virial motions and therefore that their width is suitable for virial broadening estimation without the need of introducing large corrections (Marziani et al., 2013, 2019, 2022). M_{BH} estimates remain reliable even if the effect of partially resolved outflows (in radial velocity) has to be taken into account (Negrete et al., 2018; Marziani et al., 2022; Buendia-Rios et al., 2023).

3.3 Quasar Main Sequence

3.3.1 The Eigenvector 1 / Main Sequence

The study of Boroson and Green (1992) brought together the spectral diversity of Type-1 AGNs under a single framework. Their paper is fundamental for two reasons: (i) it provides one of the first templates for fitting the Fe II pseudo-continuum. The Fe II emission manifests itself as a pseudo-continuum owing to the many, blended multiplets over a wide wavelength range, extracted from the spectrum of a prototypical Narrow Line Seyfert Type-1 (NLS1) source, I Zw 1; and more importantly, (ii) it introduced the Eigenvector 1 (E1) sequence to unify the diverse group of AGNs. They used principal component analysis – a conventional dimensionality reduction technique – on observed properties of a sample of

[†]There is a general consensus that type-1 AGN BLR gas has supersolar abundance with canonical estimates reaching over 10 times solar (Hamann and Ferland, 1993, 1999). However, the highest values depend also on the lines employed as diagnostics: the Al and Si lines are strongly dependent on enrichment by supernovae ejecta, as stressed by the authors themselves (see e.g., Garnica et al., 2022)

optically bright quasars to obtain a sequence. Of special importance is the optical plane that shows the connection between the FWHM of the broad $H\beta$ and the strength of the Fe II blend between 4434-4684 Å to the $H\beta$ (or R_{FeII}). This optical plane of the Eigenvector 1 (or of the “main sequence” of quasars) was eventually included in a 4D parameter space (4DE1) that encompasses high-ionization broad line blueshifts (Sulentic et al., 2000b, 2007), and soft-X photon index (Sulentic et al., 2000b; Bensch et al., 2015). The 4DE1 additional parameters are related to wind prominence and accretion status. It is therefore not unexpected that the main sequence might be primarily driven by the Eddington ratio i.e., the ratio between radiation and gravitational forces (e.g., Sulentic et al., 2000a; Marziani et al., 2001; Boroson, 2002; Shen and Ho, 2014; Marziani et al., 2018b) affecting several BLR physical properties (Panda et al., 2018, 2019a,c; Panda, 2021a).

3.3.2 Population A and Population B

A classification based on the width of the $H\beta$ emission line profile in an AGN spectrum was introduced by Sulentic et al. (2000a). Population A includes local NLS1s as well as more massive high accretors which are mostly classified as radio-quiet (e.g., Marziani and Sulentic, 2014a) and that have $\text{FWHM}(H\beta) \leq 4000 \text{ km s}^{-1}$. On the contrary, Population B sources are those with broader $H\beta$ ($\geq 4000 \text{ km s}^{-1}$), and are, at a large prevalence, “jetted” sources (e.g., Padovani et al., 2017). The Eigenvector 1 sequence of Boroson and Green (1992) was extended to cover the soft-X ray domain (e.g., Sulentic et al., 2000b), assessing a relation between the soft-X photon index (Γ_{soft}), the $H\beta$ line width, and the Fe II prominence (see also later developments on the relation between X-ray and optical spectra by Grupe, 2004; Grupe et al., 2010; Ai et al., 2011; Jin et al., 2012b; Bensch et al., 2015; Ojha et al., 2020).

Sources with higher values of soft X-ray excess (corresponding to a value of the soft-X photon index[‡] ($\Gamma_{\text{soft}} \approx 3 - 4$) concentrate among the highly accreting Pop. A quasars (Grupe, 2004; Sulentic et al., 2008), while Pop. B quasars typically have $\Gamma_{\text{soft}} \approx 2$. The cut-off in the FWHM of $H\beta$ at 4000 km s^{-1} was suggested by Sulentic et al. (2000a) who found that low z AGN ($z \lesssim 1$) properties appear to change more significantly at this broader line-width cutoff (see also Collin et al. 2006; Ferland et al. 2020).

The usefulness of a fixed FWHM limit – let it be 2000 km s^{-1} or 4000 km s^{-1} is questionable, as the FWHM is dependent on M_{BH} (or luminosity), viewing angle, and Eddington ratio (Marziani et al., 2018b). It makes sense if the limit is applied to samples in a narrow range of luminosity or M_{BH} . However, we reiterate the question posed a few years ago (Sulentic and Marziani, 2015):

Are populations A and B simply two extreme ends of the main sequence or do they represent two distinct quasar populations? Or are they tied via a smooth transition in the accretion mode?

The issue is very relevant to our quest to use quasars as standard, or standardizable candles, since the shape of the emission line profiles and continuum strength is directly connected to the central engine, especially to the black hole mass, and, the accretion rate, in addition to the black hole spin and, the angle at which the central engine is viewed by a distant observer (Wang et al., 2014b; Czerny et al., 2017; Marziani et al., 2018b; Panda et al., 2017, 2019c; Panda, 2021b). Looking at the black hole mass vs luminosity diagram, type-1 AGN in optically selected surveys are distributed along a relatively narrow strip with $0.01 \lesssim L/L_{\text{Edd}} \lesssim 1$, over a range of black hole masses M_{BH} exceeding 4 dexes (see e.g., the Figure 15 of D’Onofrio et al., 2021). For $L/L_{\text{Edd}} \lesssim 0.01$, accretion is expected to enter into a radiatively inefficient domain, in addition to selection effects that disfavour the lowest accretors at a given M_{BH} . At the other end of the L/L_{Edd} range, sources that radiate at $L/L_{\text{Edd}} \gg 1$ may simply not exist, as radiative efficiency is

[‡]here, the energy range considered for the estimation of the index is 0.5-2 keV based on archival Chandra and XMM-Newton data.

expected to decrease at a very high accretion rate, yielding to an asymptotic behaviour for the Eddington ratio toward a limiting value of order unity ($\sim 2 - 3$; Mineshige et al. 2000; Watarai et al. 2000; Sadowski 2011)[§]. Perhaps the following scheme is already something more than a working hypothesis: Population B is associated with modest accretion rates, and the continuum may be fit by refined α -disk models (Shakura and Sunyaev, 1973; Laor and Netzer, 1989). At some threshold of the radiative efficiency, $\eta \gtrsim 0.1$ the inner, advection-dominated region of the disk starts to have a significant role in the geometry of the BLR. At a very high accretion rate, this effect may be extreme, with collimation of ionized outflows and shielding of the low-ionization emitting region from the luminous continuum that is instead seen by an observer oriented at a small angle with respect to the disk axis (Wang et al., 2014c; Giustini and Proga, 2019, Panda and Marziani in preparation). It is also debatable to which extent accretion might be super-Eddington, as a large fraction of the infalling mass that would be accretion matter for the black hole might be actually expelled from the black hole gravitational sphere of influence (e.g., Carniani et al., 2015; Marziani et al., 2016; Vietri et al., 2018).

3.3.3 Narrow-line Seyfert 1s - a special class of AGNs?

Narrow Line Seyfert Type-1 galaxies (or NLS1s)[¶] are a class of Type-1 AGNs that are characterized with “narrower” broad emission lines: $\text{FWHM}(\text{H}\beta_{\text{broad}}) \leq 2,000 \text{ km s}^{-1}$, along with the ratio of $[\text{OIII}]\lambda 5007$ to the $\text{H}\beta$ less than 3 (Osterbrock and Pogge, 1985; Goodrich, 1989). In addition to these properties, the NLS1s often exhibit strong Fe II emission and the relative strength of the optical Fe II (within 4434-4684 Å) to the $\text{H}\beta$, or $R_{\text{FeII}} \gtrsim 1$ (Sulentic et al., 2000a; Marziani et al., 2018b; Panda et al., 2019c; Rakshit et al., 2020). NLS1s have been used to analyze the Fe II emission since the late 1970s (Phillips, 1978) and have been regarded among the most noticeable cooling agents of the BLR, emitting about $\sim 25\%$ of the total energy in the BLR (Wills et al., 1985; Marinello et al., 2016). The Fe II is a strong contaminant owing to a large number of emission lines and without proper modelling and subtraction, it may lead to a wrong description of the physical conditions in the BLR (Verner et al., 1999; Sigut and Pradhan, 2003; Sigut et al., 2004; Baldwin et al., 2004; Panda, 2021b). NLSy1s tend to be more variable than their “broader” counterparts in the X-ray regime (Grupe, 2004; Leighly, 1999; McHardy et al., 2006), although the scales of their variability are not as pronounced in the optical and infrared regime (Giannuzzo et al., 1998; Ai et al., 2013).

This is a summary of the conventional view of NLSy1s. A more exhaustive view is reached by the contextualization offered by the Eigenvector 1 Main Sequence. More prominently, the parameter R_{FeII} is central to the E1 schema as it is the dominant variable in the principal component analysis presented by Boroson and Green (1992). The PCA analysis led for the first time to the appreciation of the Fe II relevance in large samples of quasar spectra. NLSy1s showing significant Fe II emission ($R_{\text{FeII}} \gtrsim 0.5$) were described by Sulentic et al. (2000a) “as drivers of all Eigenvector 1 correlations.” Indeed, NLS1s with high accretion rates are typically shown to have a soft-X-ray excess (Arnaud et al., 1985) in their broadband SED (Jin et al., 2012a,b; Kubota and Done, 2018; Ferland et al., 2020). NLS1s also show stronger blueshifts (blueward asymmetries) especially in the HILs (e.g., Leighly and Moore, 2004; Sulentic et al., 2000a, 2007), as well as higher R_{FeII} implying high L/L_{Edd} (e.g. Du et al., 2016b). The E1 is now well understood to be associated with important parameters of the accretion process in the AGNs (Sulentic et al., 2000a; Shen

[§]Values of $L/L_{\text{Edd}} \gg 1$ should be viewed with extreme care, especially in cases of very narrow emission line profiles: orientation effects may drastically reduce the line profile in the case the emitting regions are seen pole-on. These sources stand out in a L/L_{Edd} vs M_{BH} or luminosity diagram (Marziani et al., 2006).

[¶]Type 1/Type 2 classifications are based on the observation of the broad emission line features in an AGN spectrum. According to unified model (Antonucci, 1993; Urry and Padovani, 1995; Marin, 2014; Netzer, 2015), the presence of the dusty, obscuring torus impedes/allows the direct view to the central engine of the SMBH and the BLR region – that is located closer to the SMBH. This then manifests in the AGN spectrum – where the broad emission lines originating from the BLR are either seen (Type-1) or not (Type-2).

and Ho, 2014; Marziani et al., 2018b; Panda et al., 2019c; Du and Wang, 2019; Martínez-Aldama et al., 2021), although the nature of the connection between R_{FeII} and L/L_{Edd} remains unclear to date. NLS1s typically host black holes with lower masses ($\lesssim 10^7 M_{\odot}$) and tend to be less luminous and have low radio jet power – which has led many authors (Sulentic et al., 2000a; Mathur, 2000; Fraix-Burnet et al., 2017; Berton et al., 2017) to link them to an evolutionary scheme of BHs. These authors have suggested that the NLS1s are the younger versions of more evolved, more massive SMBHs that constitute the bulk of the population of AGNs.

3.4 Accretion parameters

The estimation of black hole masses is perhaps the most sought-after analysis when it comes to AGN studies (Vestergaard and Peterson, 2006; Shen et al., 2011). AGNs show variations in their continuum and emission line intensities that can range in the order of minutes/days for the continuum to days/weeks/months timescales for the BLR region (Ulrich et al., 1997). This crucial feature led to the estimation of black hole masses for a few hundred nearby AGNs and relatively distant quasars^{||} using the technique of reverberation mapping (Blandford and McKee, 1982; Peterson et al., 2004a; Peterson, 1988, 1993) with the knowledge of the location of the line emitting region from the central SMBH^{**}. Coupling the information of the velocity broadening from single/multi-epoch spectroscopy (Bentz et al., 2013; Du et al., 2014; Kaspi et al., 2000) with a basic knowledge of the geometry of the emitting region (Pancoast et al., 2014; Li et al., 2016, 2018), we are well poised to derive the black hole masses using the virial relation (Peterson et al., 2004b): $M_{\text{BH}} \sim f_{\text{S}} r_{\text{BLR}} \delta v^2 / G$. There remains still a considerable level of uncertainty in the virial factor f_{S} (Marziani and Sulentic, 2012; Shen, 2013): the geometry and dynamics of the emitting regions remain poorly constrained. In dealing with M_{BH} estimate we actually encounter several difficulties associated with the lack of spherical symmetry of the BLR velocity field (McLure and Jarvis, 2002; Decarli et al., 2011), and with the possibility of anisotropic continuum emission. The uncertainties in the M_{BH} estimation affect the L/L_{Edd} estimates as well, with the complication that L/L_{Edd} estimates from optical/UV data depend on a bolometric correction that in turn depends not only on accretion state as evinced from Figure 1 but also on luminosity (e.g., Netzer, 2019, and references therein) as well as on viewing angle (e.g., Runnoe et al., 2013). Curiously, if the assumption of a highly flattened H β emitting region is correct, there could be a way out right for super-Eddington sources exploiting the computation of the “virial luminosity” from line widths (Section 4 and Eq. 1).

The ratios between the virial and the redshift-based luminosity can be explained entirely by orientation effects (Negrete et al., 2018), thereby making it possible to derive an estimate of the viewing angle for each individual source. This method has been barely explored, but it has in principle the ability to constrain the disk/wind scenario in extreme Population A. We will discuss in §4.3 the anisotropy in continuum emission for xA sources - these refer to the sources that exhibit strong Fe II emission ($R_{\text{FeII}} \gtrsim 1$) and are associated with accretion rates close to the Eddington limit, in the optical plane of the Eigenvector 1 main sequence diagram (Marziani et al., 2018a; Panda et al., 2019c).

4 AN AVENUE FOR COSMOLOGICAL STUDIES?

A better understanding of the AGN’s inner workings can pave the road to far-reaching applications. One of them is the standardization of quasars (or QSOs) for measuring cosmological parameters. Two methods

^{||}Quasars, or QSOs, are luminous AGNs discovered at larger redshifts. This distinction is mainly of historical importance; in the following, we will use the term quasars as an umbrella term for type 1 AGN.

^{**}In actuality, the difference in the light travel time is estimated by making a cross-correlation between the continuum light directly reaching us and the light that bounces first at the BLR region and then comes to us (Peterson, 1993; Horne et al., 2004). The continuum light is produced very close to the SMBH – in correspondence with the inner accretion disk (see e.g., Shakura and Sunyaev, 1973; Czerny and Elvis, 1987).

that involve quasar intrinsic properties resort to a law analogous to that of Faber-Jackson, connecting velocity dispersion and luminosity (Section 4.1), and the radius-luminosity scaling laws (Section 4.2). Both methods face challenges.

4.1 Eddington standard candles?

The application of quasars radiating at or above the Eddington limit has been proposed for several years although the method has not yet been exploited to its full potential (Marziani et al., 2021b; Dultzin et al., 2020, and references therein). The method is conceptually simple: the accretion luminosity of a quasar is proportional to a power of the line width^{††}, i.e., $L \propto \text{FWHM}^n$. The value of the exponent $n = 4$ comes from the virial relation for the black hole mass, the assumptions of constant Eddington ratio ($L/L_{\text{Edd}} \propto L/M_{\text{BH}} \approx \text{const.}$), and of BLR radius rigorously scaling with luminosity as $r \propto L^{0.5}$. The last assumption is likely to be verified for sources radiating close to the Eddington limit: they are identified by spectral similarity ($R_{\text{FeII}} > 1$), and so SED and the physical properties of the emitting regions need to be similar.

More in detail, the equation connecting luminosity and line width can be written as:

$$L \sim \mathcal{L}_\bullet \eta^2 f_S^2(\theta) \mathcal{S}(\text{SED}) \frac{1}{\mathcal{P}} \delta v_r^n \quad (1)$$

where we have evidenced the main physical factors entering the estimate of the virial luminosity from measurements of radial velocity dispersion δv_r (FWHM, σ). The effect of orientation can be quantified by assuming that the line broadening is due to an isotropic component δv_{iso} + a flattened component whose virial velocity field projection along the line of sight is

$$\delta v_r^2 = \frac{\delta v_{\text{iso}}^2}{3} + \delta v_K^2 \sin^2 \theta. \quad (2)$$

that implies:

$$f_S(\theta) = \frac{1}{\frac{1}{3} \left(\frac{\delta v_{\text{iso}}}{\delta v_K} \right)^2 + \sin^2 \theta} \quad (3)$$

The factor \mathcal{S} is the ratio between the SED fraction of the ionizing continuum and the average energy of the ionizing photons. The factor \mathcal{P} is the product density times ionization parameter ($n_{\text{H}} U \sim 10^{9.6} \text{cm}^{-3}$, Padovani and Rafanelli 1988; Matsuoka et al. 2008; Negrete et al. 2012). The two factors come from the definition of the photoionization radius of the BLR (Wandel et al., 1999). Deviations between the virial estimates and luminosity estimated from redshift and assumed concordance cosmology can be fully explained by the effect of orientation (Negrete et al., 2018). The distributions of the viewing angles from the Negrete et al. (2018) sample based on $\text{H}\beta$ at low z peaks at about 17 degrees, with only a very small fraction of quasars, is observed at $\theta \gtrsim 30^\circ$. This means that the effect of kinematic anisotropy on the computation of the virial luminosity should introduce a significant dispersion, as it is $\propto 1/\sin^2 \theta$.

4.2 Scatter in the R-L relation, standardizing QSOs for cosmological studies

An important result of the reverberation mapping studies is from the empirical power-law relation between the BLR radius (or light travel time delay) and the luminosity, $R_{\text{BLR}} \approx c\tau \propto L_{5100}^\alpha$, where τ is the time

^{††}The equation is equivalent to the original formulation of the Faber-Jackson law (Faber and Jackson, 1976) and is equivalent to other relations linking virialized systems to the amount of radiation emitted.

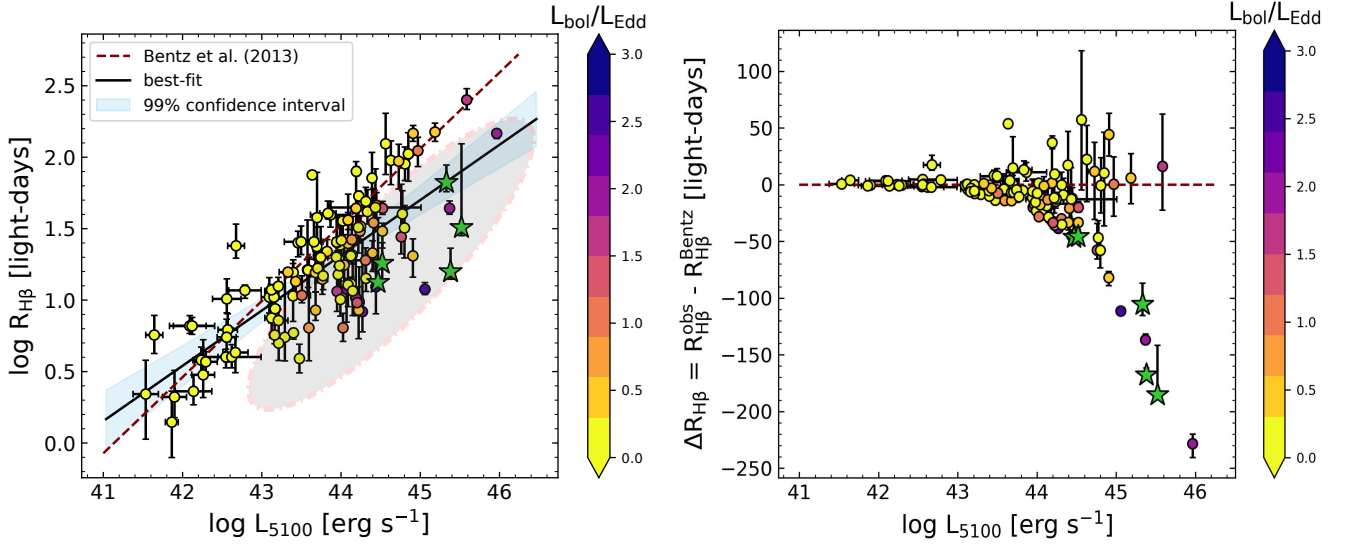


Figure 2. (Left:) BLR radius (of $H\beta$ emitting region) versus the AGN monochromatic luminosity at 5100\AA . The sources are coloured with respect to their Eddington ratios (L_{bol}/L_{Edd}). The dashed line shows the classical relation from Bentz et al. (2013). The linear best-fit relation (black solid line) for the sources has the form: $\log R_{H\beta} = 0.387 \times (\log L_{5100}) - 15.702$, with a Spearman’s correlation coefficient $\rho \approx 0.733$ and p-value $\approx 2.733 \times 10^{-21}$. The shaded region in light blue marks the 99% confidence interval about the linear best-fit relation. The shaded ellipse highlights the sources with relatively high Eddington ratio values that deviate away from the classical relation, i.e., towards shorter BLR radii. Sources with $L/L_{Edd} > 3$ are highlighted using star symbols in green. Data are from Martínez-Aldama et al. (2019) which compiled the observational data for the 117 AGNs that consists of 48 sources previously monitored by Bentz et al. (2009, 2014), Barth et al. (2013), Pei et al. (2014), Bentz et al. (2016), and Fausnaugh et al. (2017), 25 super-Eddington sources of the SEAMBH project (Super-Eddington Accreting Massive Black Holes, Wang et al., 2014a; Du et al., 2015; Hu et al., 2015; Du et al., 2016a, 2018), 44 sources from the SDSS-RM (Grier et al., 2017) sample and the recent monitoring for NGC5548 (Lu et al., 2016) and 3C273 (Zhang et al., 2019). (Right:) The difference between the observed time delay (as shown with the data points in the left panel) and the time delay predicted by the classical relation from Bentz et al. (2013). Here, the dashed line represents the null difference between the two delays.

delay in response to continuum variation of a suitable line, mostly $H\beta^{\ddagger\dagger}$. Bentz et al. (2013) found a best-fit for a sample of 41 AGNs covering four orders of magnitude in luminosity with a power-law slope value, $\alpha = 0.533^{+0.035}_{-0.033}$, very close to the theoretical value, $\alpha = 0.5$ needed to preserve spectral similarity (Wills et al., 1985; Davidson, 1977; Osterbrock and Ferland, 2006). This function is shown using a dashed line in the left panel of Figure 2. One can then combine the R_{BLR} - L_{5100} relation with the line widths for the broad emission lines estimated from single/multi-epoch spectroscopy to estimate the black hole masses which makes it especially useful for large statistical surveys of sources throughout cosmic history (Vestergaard and Peterson, 2006; Shen et al., 2011).

Recent observations have led to populate the R_{BLR} - L_{5100} observational space and take the total count over 100, especially the sources monitored under the SEAMBH project (Super-Eddington Accreting Massive Black Holes, Du et al. 2014; Wang et al. 2014a; Hu et al. 2015; Du et al. 2015, 2016a, 2018), and from the SDSS-RM campaigns (Grier et al., 2017; Shen et al., 2019). But this has introduced us to a new challenge - the inherent dispersion in the R_{BLR} - L_{5100} relation after the introduction of these new sources. The left panel of Figure 2 is an abridged version from Martínez-Aldama et al. (2019); Panda

^{††}Here, the relation assumes the BLR radius for the $H\beta$ and the nearest continuum luminosity at 5100\AA

(2021a) where the $R_{\text{BLR}}\text{-}L_{5100}$ observational space for 117 reverberations mapped AGNs is shown. The sources are coloured with respect to their Eddington ratios ($L_{\text{bol}}/L_{\text{Edd}}$). The best-fit relation for this sample is, $\log R_{\text{H}\beta} = 0.387 \times (\log L_{5100}) - 15.702$, with a Spearman's correlation coefficient (ρ) = 0.733 and $p\text{-value} = 2.733 \times 10^{-21}$, thus making the overall slope of the relation much shallower than obtained from the previous studies by Bentz et al. (2013) and bringing the validity of the empirical $R_{\text{BLR}}\text{-}L_{5100}$ relation into question. But interestingly, the sources that eventually led to the increase in the scatter in the relation show a trend with the Eddington ratio - the larger the dispersion of a source from the empirical $R_{\text{BLR}}\text{-}L_{5100}$ relation, the higher its Eddington ratio! In Martínez-Aldama et al. (2019), we found that this dispersion can be accounted for in the standard $R_{\text{BLR}}\text{-}L_{5100}$ relation with an added dependence on the Eddington ratio ($L_{\text{bol}}/L_{\text{Edd}}$). This is highlighted in the right panel of Figure 2, where the difference between the observed time delays and that estimated from the empirical $R_{\text{BLR}}\text{-}L_{5100}$ relation (i.e., ΔR_{BLR} , Bentz et al., 2013), for the sources shown in the left panel, are plotted against their respective L_{5100} . One can appreciate the drop in the ΔR_{BLR} value, especially for sources with high Eddington ratios indicating that sources with shorter 'observed' time lag especially at the high luminosity end of the scaling relation exhibit high accretion rates. In other words, these sources are expected to host SMBHs with low BH masses (Du et al., 2014, 2016a). Although we note that there are some sources which, albeit being of high Eddington nature, are observed to have R_{BLR} sizes comparable to the predicted value from Bentz et al. (2013). Du and Wang (2019) exploited this further in their work and realized that with an additional correction term, the relation can be reverted back to the original relation with a slope ~ 0.5 . This additional correction term is an observational parameter, the relative strength between the optical Fe II emission and the corresponding H β emission (R_{FeII}) that has been shown in earlier studies to be a reliable observational proxy for the Eddington ratio (Sulentic et al., 2000a; Marziani et al., 2001; Shen and Ho, 2014; Marziani et al., 2018b; Panda et al., 2019c; Du and Wang, 2019; Martínez-Aldama et al., 2021) which we touched upon in earlier sections. The relation takes the form (Du and Wang, 2019):

$$\log \left(\frac{R_{\text{BLR}}}{1 \text{ light-day}} \right) = \kappa + \alpha \log \left(\frac{L_{5100}}{10^{44} \text{ erg s}^{-1}} \right) + \gamma R_{\text{FeII}} \quad (4)$$

where the flux (F) can be independently estimated from the observed AGN spectrum for a given source. With this correction in terms of an observable quantity, i.e., R_{FeII} , we avoid the circularity problem which was present when the correction was explicitly made in terms of the Eddington ratio (Martínez-Aldama et al., 2019), and can have a robust estimate of the luminosity distance (D_L). This then allows us to construct a Hubble diagram using quasars where we know their luminosity distance and their redshifts, and test the validity of the standard cosmological model and their alternatives (see e.g. Haas et al., 2011; Watson et al., 2011; Czerny et al., 2013, 2019, 2021; Zajaček et al., 2021; Khadka et al., 2021, 2022). Super-Eddington accreting sources are expected to be preferentially selected with increasing redshift in flux-limited sample (Sulentic et al., 2014). A combination of this selection bias and intrinsic Eddington ratio evolution (e.g., Cavaliere and Vittorini, 2000; Hopkins et al., 2006) makes for high redshift quasar spectra often resembling lower- z extreme Population A spectra (an effect predicted by Sulentic et al. 2000a). Their inclusion is thus vital in extending the $R_{\text{BLR}}\text{-}L_{5100}$ relation to higher luminosity regime as shown in Figure 3. where, $\kappa=1.65 \pm 0.06$, $\alpha=0.45 \pm 0.03$, and $\gamma=-0.35 \pm 0.08$. Clearly, the introduction of the R_{FeII} term and for sources with strong Fe II emission, is able to account for their shorter time-lags and hence, smaller R_{BLR} sizes. In addition, we are able to recover the slope (α) closer to the theoretical predictions, i.e., 0.5 (Davidson, 1977; Davidson and Netzer, 1979) and hence, we can safely use the modified $R_{\text{BLR}}\text{-}L_{5100}$ relation (including the correction term wrt R_{FeII}) to independently estimate the monochromatic luminosity

for a given source, and couple the information from the flux obtained from direct observations, to eventually estimate the luminosity distance to the said source:

$$D_L = \sqrt{L_{5100}/4\pi F} \propto \frac{c\tau}{\sqrt{4\pi F}} \quad (5)$$

where the flux (F) can be independently estimated from the observed AGN spectrum for a given source. In this way, we can avoid circularity and can have a robust estimate of the luminosity distance.

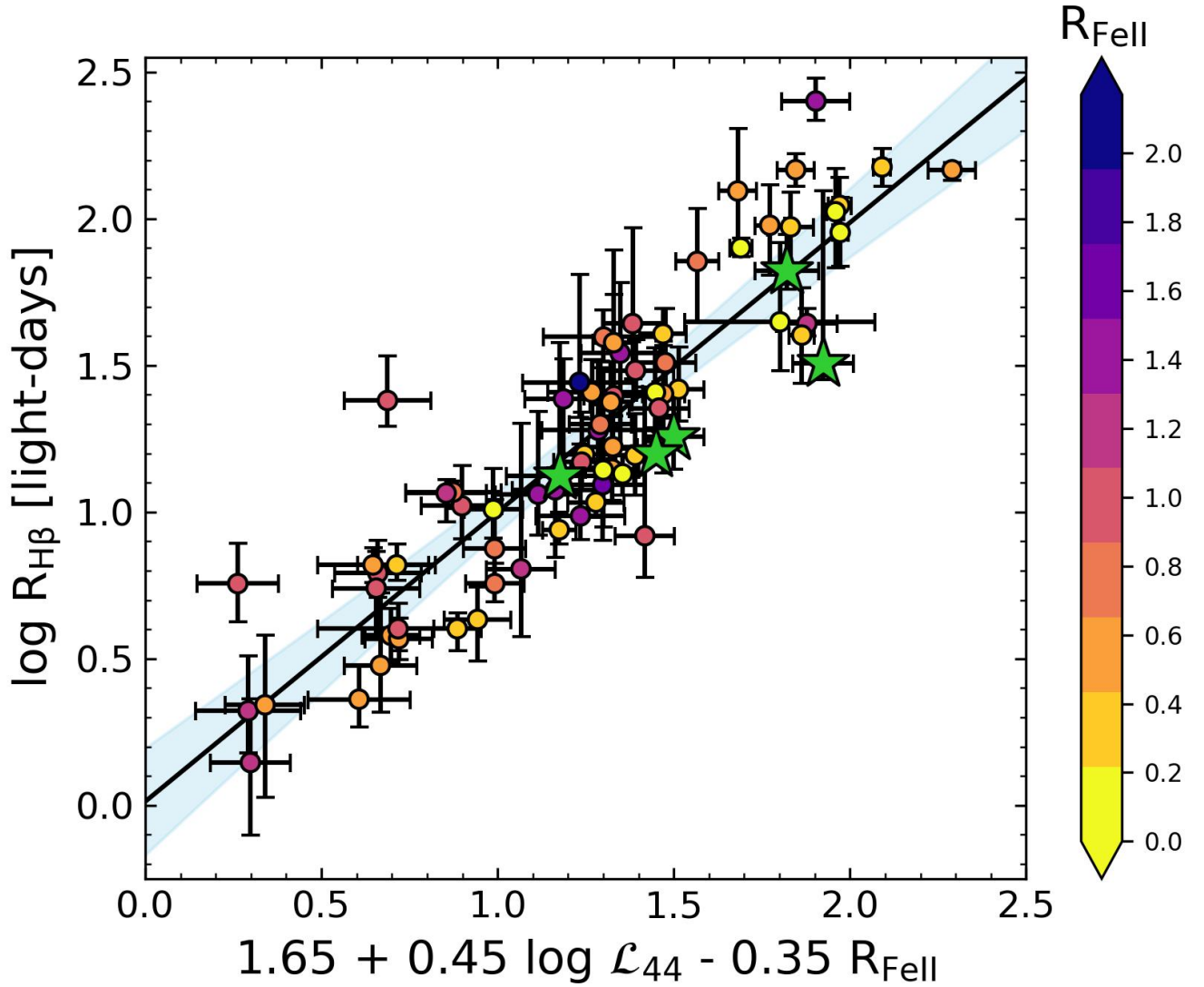


Figure 3. An abridged version of Figure 5 in Du and Wang (2019) showing the new $R_{\text{BLR}} - L_{5100}$ relation with the inclusion of the R_{FeII} . The sample contains 75 reverberation-mapped sources which have R_{FeII} estimated from their respective spectrum. The best-fit relation is shown in a black solid line with $\rho = 0.894$ and $p\text{-value} = 3.466 \times 10^{-27}$. The corresponding shaded region (in light blue) highlights the 99% confidence interval about the linear best-fit relation with an effective scatter of ~ 0.196 dex. Here, \mathcal{L}_{44} represents the L_{5100} normalized by $10^{44} \text{ erg s}^{-1}$ consistent with the formalism of Du and Wang (2019). Sources with $L/L_{\text{Edd}} > 3$ are highlighted using star symbols in green as shown in Figure 2.

4.3 Anisotropic radiation from the accretion disk

An equally important aspect in this regard is the ionizing continuum produced by the central engine. The characterization of the ionizing SED that comes from regions closer than the BLR is important for our study of the emission lines. From the photo-ionization point of view, this fraction of the broad-band SED is closely related to the number of ionizing photons that eventually leads to the line production that has permitted the estimation of a photoionization radius of the BLR (Wandel et al., 1999; Negrete et al., 2014; Martínez-Aldama et al., 2015; Panda, 2021b, 2022).

We tested the variation in the low-ionization part of the BLR by accounting for the changes in the shape of the ionizing continuum (the SED) and the location of the $H\beta$ -emitting BLR from the central ionizing source (or R_{BLR}) from the reverberation mapping, in the context of Main Sequence of Quasars (Panda, 2022). In this and previous work (Panda, 2021b), we have found that in order to estimate the correct physical conditions for these low-ionization lines emitting regions in the BLR, it is not sufficient to only retrieve the flux ratios (e.g., R_{FeII}) but to also have an agreement with the corresponding modelled and observed line strengths (or line equivalent widths, EWs). Compared to the results that are directly obtained from the photoionization theory, these new results highlight the shift in the overall location of the line-emitting R_{BLR} - in terms of the ionization parameter U and the local cloud density (n_{H}) recovered from the analysis towards lower values (by up to 2 dexes) compared to the R_{BLR} values estimated from the photoionization theory. This brings the modelled location in agreement with the reverberation mapping results, especially for the high-accreting NLS1s which show shorter time-lags/smaller emitting regions. A corollary result is that to retrieve such physical conditions, the BLR should “see” a different, filtered SED with only a fraction of the total ionizing photon flux. This analysis was performed on selected sources with readily available broad-band SEDs and archival spectroscopic measurements. In addition, we assumed source-specific metallicities that were derived using the UV diagnostic lines from earlier studies (see e.g., Marziani et al., 2022). There is a need to extend this analysis to a larger number of reverberation-mapped sources. We, therefore, need synchronous multi-wavelength observations to build robust SEDs that can be used to confirm this scenario. Also, there is a need to bring together a global picture where a combined analysis of the UV and optical emitting regions can be put together – to allow us to gauge the salient differences in the low- and high-ionization line emitting regions.

Wang et al. (2014c) derived the analytical solutions (steady-state) for the structure of “slim” accretion discs from sub-Eddington accretion rates to extremely high, super-Eddington rates. They notice the appearance of a funnel-like structure very close to the SMBH at super-Eddington rates and attribute this feature to the puffing up of the inner accretion disk by radiation pressure, wherein the Shakura and Sunyaev (1973) prescription for a geometrically thin, optically thick accretion disk does not hold (Abramowicz et al., 1988; Sadowski, 2011; Wang et al., 2014c). We show an illustration of this scenario in Figure 4. Such modifications to the disk structure strongly affect the overall anisotropic emission of ionizing photons from the disk in addition to just inclination effects that arise due to the axisymmetric nature of these systems. Therefore, with a rise in accretion rates, a continuum anisotropy needs to be accounted for. The anisotropy then leads to the shrinking in the position of the BLR – exposed to a lower continuum flux than the observer (Figure 4) – that brings the modelled location in agreement with the observed estimates from the reverberation mapping campaigns (see Panda, 2021b, for more details).

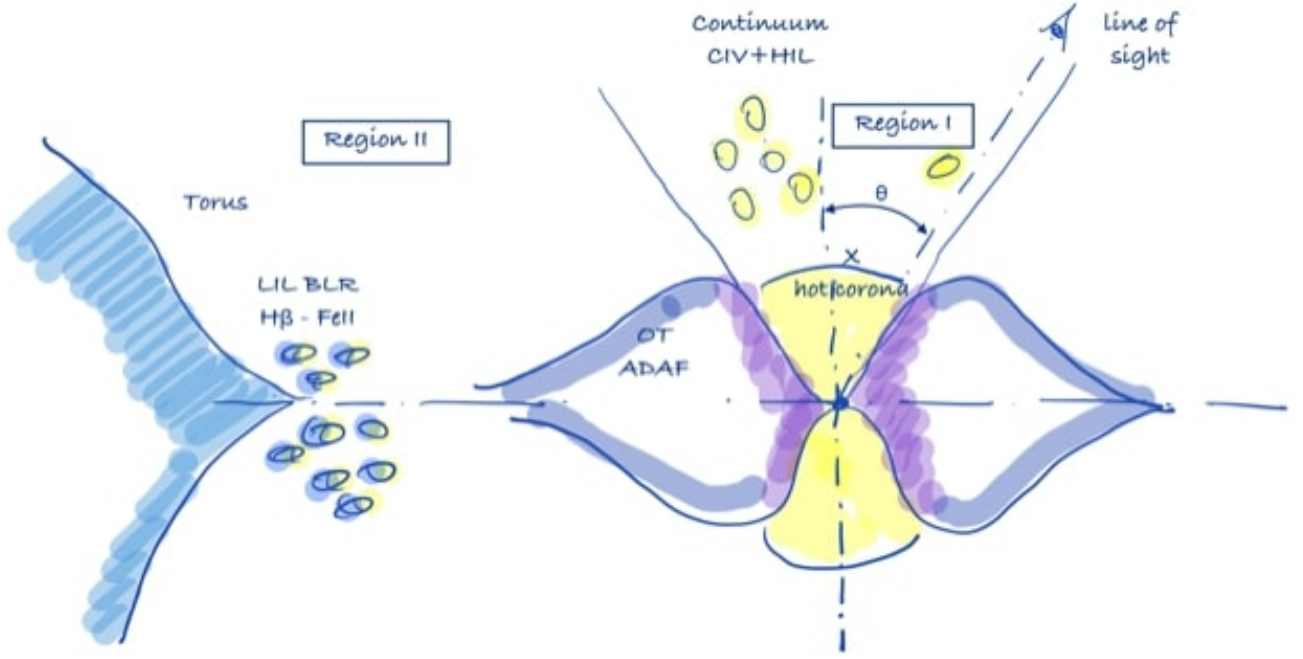


Figure 4. Schematic view of the inner sub-parsec region around the SMBH for a high accreting AGN. Region I is exposed to the continuum emitted from the hottest part of the optically thick (OT) and geometrically thick advection-dominated accretion flow (ADAF). The observer sees inside of this region if the line-of-sight is inclined by $\lesssim 30$ degrees from the disk axis. Region II refers to the region shielded from the hottest region and exposed to a colder continuum emitted from the ADAF at angles $\gtrsim \theta$. Abridged version from Wang et al. (2014c); not drawn to scale.

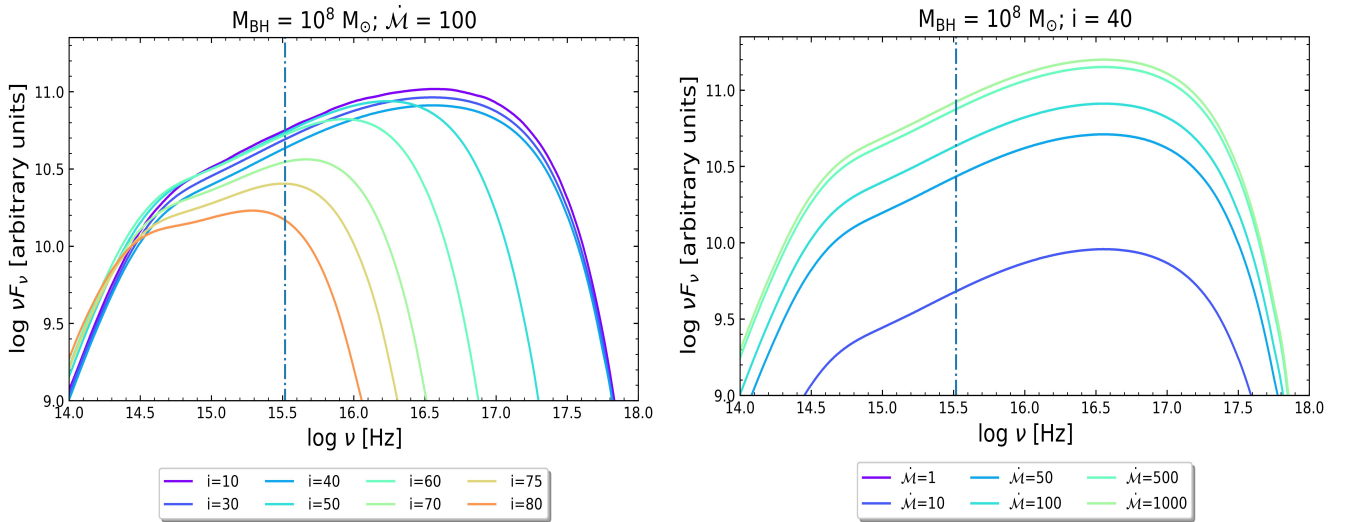


Figure 5. Spectral energy distributions (SEDs) obtained for slim accretion disks for a representative black hole mass, $M_{\text{BH}} = 10^8 M_{\odot}$. LEFT: SEDs are shown for a range of viewing angle cases for a representative dimensionless accretion rate, $\dot{M} = 100$. RIGHT: SEDs are shown for a range of \dot{M} for a representative viewing angle, $i = 40^\circ$. In both panels, the vertical dash-dotted line marks the 1 Rydberg threshold.

The left panel in Figure 5 shows the slim-disk SEDs (Jian-Min Wang, priv. comm.) for a representative BH mass of $10^8 M_{\odot}$, accreting at $\dot{M} = 100$ for a range of viewing angles^{§§}. The right panel shows the

^{§§}This is the dimensionless accretion rate introduced by Wang et al. (2014a): $\dot{M} = \dot{M}/\dot{M}_{\text{Edd}}$, with $\dot{M}_{\text{Edd}} = L/c^2$, and \dot{M} the mass accretion rate. In Panda (2022) we provide an analytical form to convert \dot{M} to Eddington ratio ($L_{\text{bol}}/L_{\text{Edd}}$, see equation 13 in their paper). This relation additionally depends on the BH mass and the bolometric correction. For a BH mass of $10^8 M_{\odot}$ with $\dot{M} = 100$, for a $L_{5100} = 10^{45} \text{ erg s}^{-1}$, the Eddington ratio is ~ 0.1 .

Table 1. Fraction of ionizing continuum flux (in %) of the slim disk SED shown in the left panel of Figure 5 (relative to the case with $i = 10^\circ$)

i	ratio (%)
10°	100.00
30°	87.91
40°	77.92
50°	26.11
60°	7.95
70°	1.91
75°	0.78
80°	0.23

Table 2. Fraction of ionizing continuum flux (in %) under the slim disk SEDs shown in the right panel of Figure 5 (normalized to the case with $\dot{M} = 1000$)

\dot{M}	ratio (%)	ratio \dot{M}_i / ratio \dot{M}_{i-1}
1	0.44	...
10	5.71	12.98
50	32.40	5.67
100	51.49	1.59
500	89.48	1.74
1000	100.00	1.12

distribution of slim-disk SEDs as a function of \dot{M} for a representative BH mass of $10^8 M_\odot$ observed at a viewing angle ($i = 40^\circ$). We also report the relative area under the SEDs shown in Figure 5. These values are tabulated in Tables 1 and 2 corresponding to the left and right panels of Figure 5, respectively. We estimate the area under the SEDs accounting only for the fluxes corresponding to a frequency ≥ 1 Rydberg^{¶¶}. We then compute the relative area (a) with respect to the SED case with the viewing angle, $i = 10^\circ$ (Table 1 and left panel of Figure 5); and (b) with respect to the SED case with the dimensionless accretion rate, $\dot{M} = 1000$ (Table 2 and right panel of Figure 5). From the left panel of Figure 5, we can notice that going from the SED viewed at $i = 10^\circ$ to 80° , keeping the BH mass and accretion rate constant, the extended region II receives only a very small fraction of the actual *ionizing* photon flux (only 0.23%), meaning almost all of the ionizing photons (99.77%) never make it to the BLR. This ~ 2 dex reduction in the photon flux results in an equal reduction in the ionization parameter (U) which was confirmed already in Panda (2021b). On the other hand, changing the accretion rate, going from $\dot{M} = 1$ to 1000 and keeping the BH mass and viewing angle constant (right panel of Figure 5), we find that an accretion rate $\dot{M} = 1$ relates to only a 0.44% of the total photon flux, also a factor $\gtrsim 100$ from the case $\dot{M} = 1000$. There is however a fundamental difference: whereas changing \dot{M} produces an almost self-similar shift of the SED, a change in the viewing angle produces the change by a factor $\gtrsim 100$ in the *ionizing flux*, while the optical flux changes by a factor $\approx a few$ (Figure 5). This indirectly confirms the results of previous works that have been pointing to the main sequence drive being the Eddington ratio convolved with the effect of orientation (Marziani et al., 2001; Shen and Ho, 2014; Sun and Shen, 2015; Marziani et al., 2018b; Panda et al., 2019c). The shape of the SED thus plays an important role in explaining the trends in the quasar main sequence wherein the information of the fundamental BH parameters – BH mass, Eddington ratio, orientation and the BH spin – are embedded (see Panda, 2021a, for more details).

^{¶¶} 1 Rydberg $\approx 3.29 \times 10^{15}$ Hz

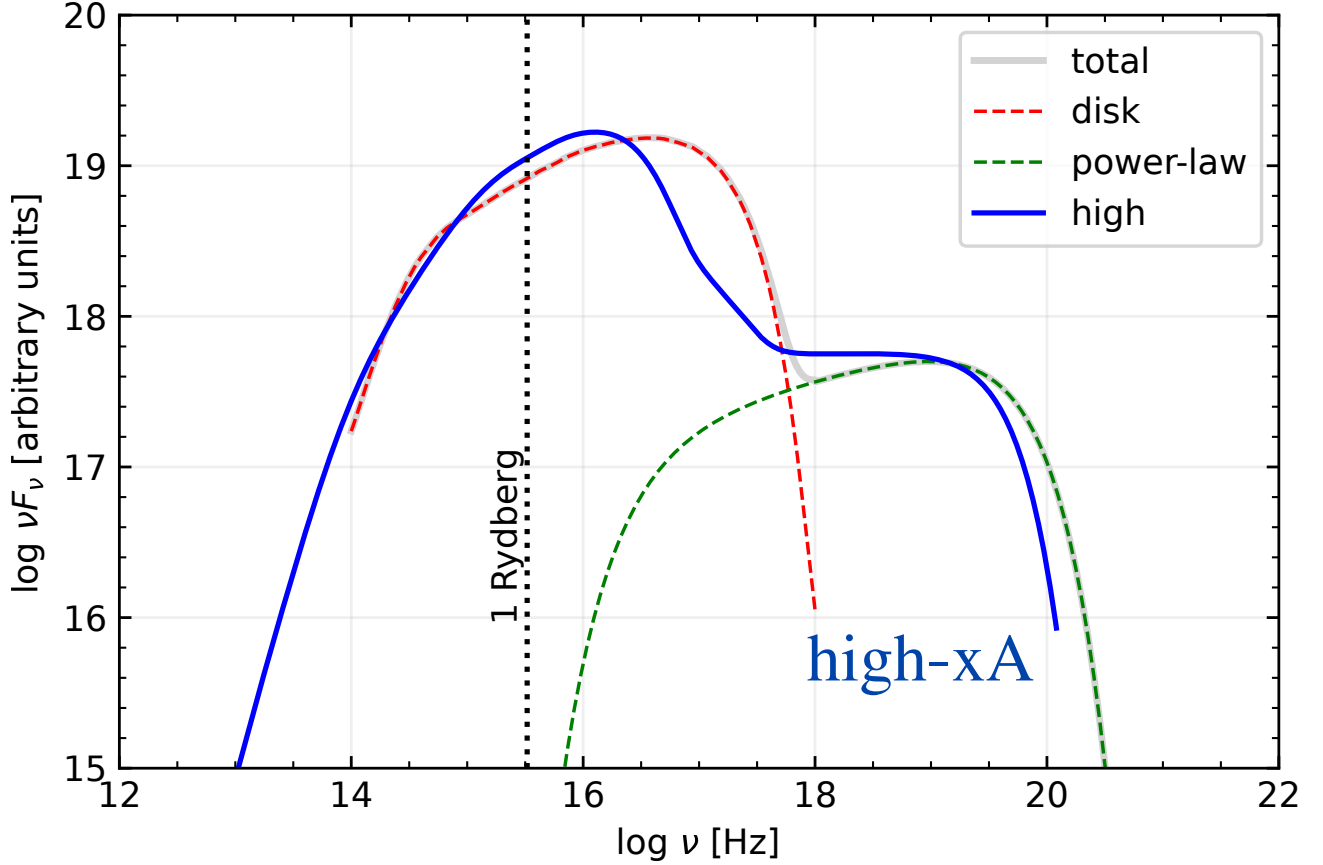


Figure 6. A simplified model for the “high” SED of Ferland et al. (2020) using the $\dot{M} = 500$ SED from Wang et al. (2014c) and an X-ray emitting corona (power law with exponential breaks). Note that the high-energy turnover at $\log \nu \sim 20$ [Hz] is actually poorly known, and in the most extreme case, the hard X-ray SED may show no flattening and no break (“highest” case; magenta line in Figure 1).

In Figure 6, we highlight a representative fit (in grey) to the high SED case (in blue) from Ferland et al. (2020) utilizing a two-component model, i.e., a slim accretion disk that represents the thermal component (in dashed red) along with a hot Comptonized component (in dashed green). Here, the slim accretion disk SED is modelled for a face-on viewing angle, $i = 10^\circ$ for a $\dot{M} = 500$ for a BH mass of $10^8 M_\odot$. The X-ray to optical-UV normalization is set by a spectral index ($\alpha_{\text{ox}} = -1.47$) and the high-energy cutoff is assumed to be ~ 2.5 keV with a slope ($\alpha_x = -0.79$) to match the exponential drop in the observed SED. The assumed values for these parameters are considered from Jin et al. (2012a,b) who were the first to carry out a broadband analysis on these composite SEDs. This instance of the slim accretion disk SED is a good fit for xA as shown in Figure 7 where the latter is represented by a composite spectrum made using the optical-UV spectral observations for xA sources from Marziani et al. (2013). In our forthcoming work, we will incorporate these slim disk SEDs into our photoionization modelling setup and recover the trends for the low- and high-ionization emission lines, their relative strengths (e.g., R_{FeII}) and the EWs, concerning these fundamental BH parameters, concentrating on the xA.

Table 2 shows that the fraction of ionizing photons at a very high accretion rate tends to saturate, with only a 10% increasing from the doubling of the accretion rate, from $\dot{M} = 500$ to 1000. At such \dot{M} the Eddington ratio should converge toward a limiting value of $\mathcal{O}(1)$. The product $n_{\text{H}}U$ is also little affected by

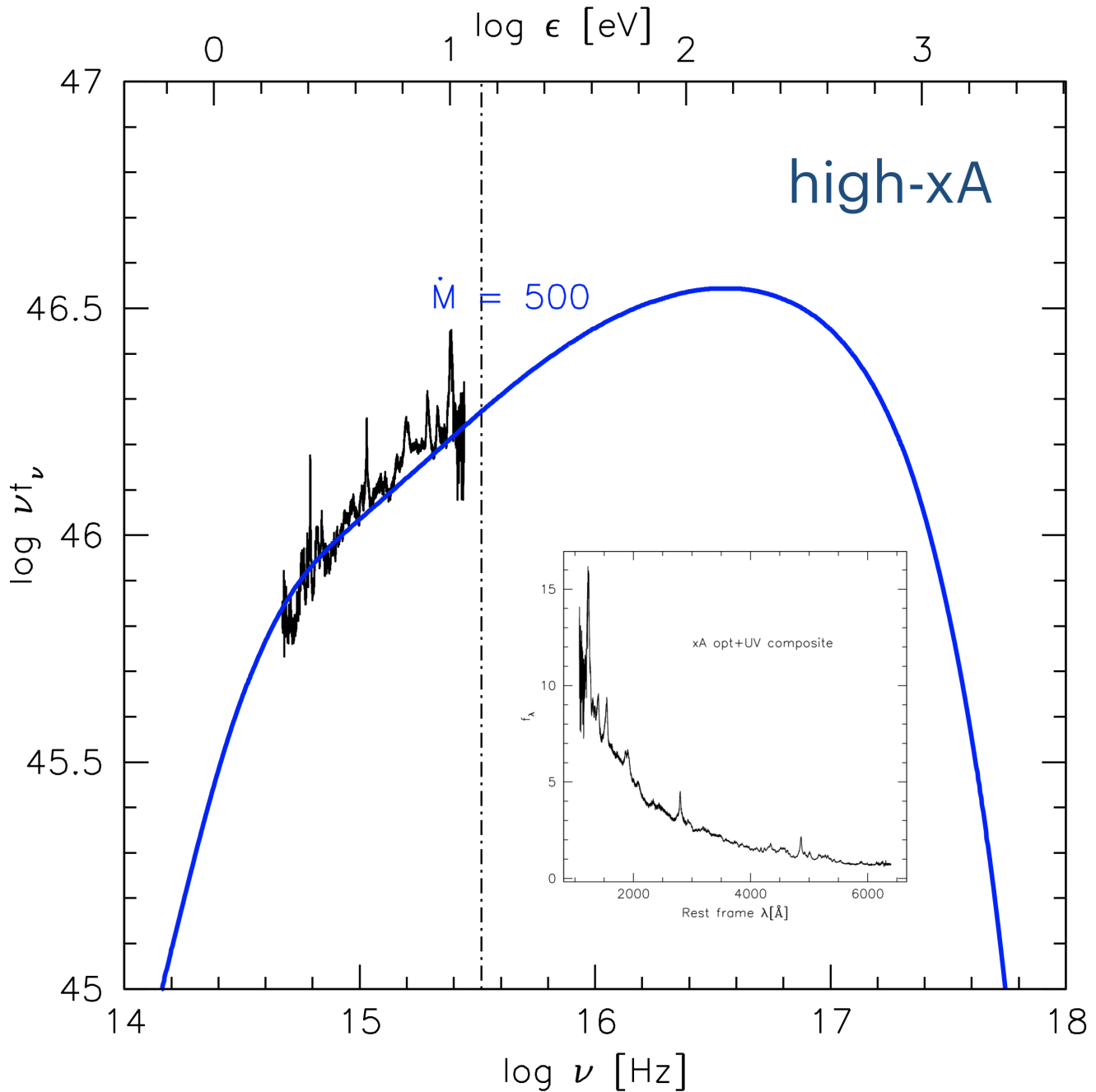


Figure 7. Composite spectrum for xA from Marziani et al. (2013), with the Wang et al. (2014c) SED superimposed for $\dot{M} = 500$. The inset shows the same spectrum as a function of wavelength.

changes in SED in the cases shown in Figure 1. The factors \mathcal{S} and \mathcal{P} are expected to be stable,^{***} although their actual dispersion and systematics for sources selected as radiating closer to the Eddington limit should be further investigated through dedicated observations. In other words, even if anisotropy effects in line widths are strong, anisotropy in continuum emission and differences in SEDs might not be so strong as to compromise an application to the cosmology of Eq. 1 that is – we stress it – generally valid for all AGNs but in practice exploitable for high accretors only. Preliminary applications to cosmology of Eq. 1 have

^{***}The average frequency of the ionizing continuum changes by just 5% passing from the Mathews and Ferland (1987) to Marziani and Sulentic (2014a): from $\langle h\nu \rangle \approx 3.03$ to $\langle h\nu \rangle \approx 3.17$ Ryd.

been encouraging (Marziani and Sulentic, 2014a,b; Marziani et al., 2019; Czerny et al., 2021; Marziani et al., 2021b,a).

5 CONCLUDING REMARKS

We have reviewed some basic aspects of luminous type-1 AGN (Section 1) to introduce highly accreting sources with special attention to their SEDs (Section 3), focusing on the most relevant aspects (such as anisotropy, Sect. 4.3) in the context of the possible application to the measurements of the cosmological parameters (Sections 3 and 4). We have stressed that Population A includes NLS1s but that only a fraction of the sources can be considered highly accreting, as a defining criterion is $R_{\text{FeII}} \gtrsim 1$, and this criterion is not met by all Population A and NLS1 sources. On the converse, a criterion based on line width implies a dependence on black hole mass (and hence luminosity in flux-limited samples), viewing angle, Eddington ratio, and yields a selection that is, unavoidably, sample dependent (Marziani et al., 2018a; Panda et al., 2019c).

Looking at the bigger picture, we can construct the Hubble diagram with the luminosity distances using Eq. 5 corrected according to Eq. 4 and the corresponding redshifts for each source. The key here is to have the measurement of the time-delay (e.g., from Eq. 4) and the AGN monochromatic flux using single epoch spectra that allow us to estimate the luminosity distances regardless of accretion properties. Hence, very large samples of reverberation-mapped AGNs can be used as cosmological candles (Collier et al., 1999; Elvis and Karovska, 2002; Horne et al., 2003; Panda et al., 2019b; Khadka et al., 2022). This may further allow us to study the evolution of the cosmological parameters as a function of the redshift allowing for the reconciliation of the Hubble tension - the disparity between the measured value of the Hubble constant in the local and the early Universe (see Figure 8).

There will be an immense potential for the ideas and results presented in this work in the near future, serving as test-beds for the vast number of AGNs that will be explored with the ongoing and upcoming ground-based 10-metre-class (e.g. Maunakea Spectroscopic Explorer, Marshall et al., 2019) and 40 metre-class (e.g. The European Extremely Large Telescope, Evans et al., 2015) telescopes; and space-based missions such as the JWST (Gardner et al., 2006; Jakobsen et al., 2022) and the Nancy Grace Roman Space Telescope (Spergel et al., 2013). Increased availability of high-quality, multi-wavelength photometric, spectroscopic and interferometric measurements extending to higher redshifts is a necessity to help develop our ever-growing theoretical understanding of how these massive, energetic cosmic sources work and evolve as well as how they might be exploited for cosmic distance estimates.

CONFLICT OF INTEREST STATEMENT

The author declares that the research was conducted in the absence of any commercial or financial relationships that could be construed as a potential conflict of interest.

AUTHOR CONTRIBUTIONS

All authors listed have made a substantial, direct, and intellectual contribution to the work and approved it for publication.

FUNDING

ACKNOWLEDGMENTS

SP acknowledges the Conselho Nacional de Desenvolvimento Científico e Tecnológico (CNPq) Fellowship (164753/2020-6). SP further acknowledges the organizers of the SPIG - 31st Summer School and

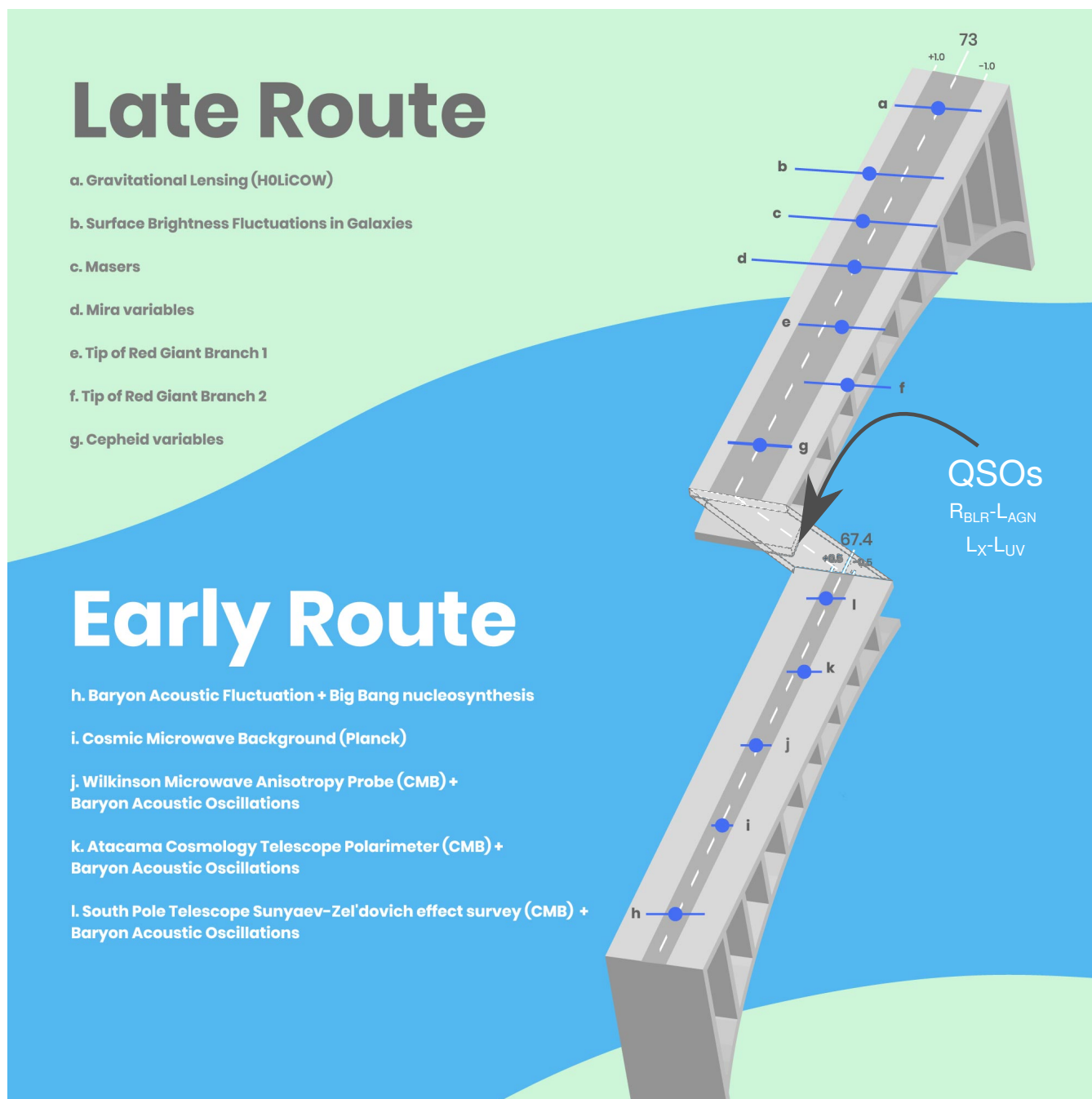


Figure 8. This graphic lists the variety of techniques that have been used to measure the expansion rate of the universe, known as the Hubble constant (H_0). One set of observations looked at the very early universe (or the early route, shown in the bottom half of the graphic) and the second set of observation strategies analyzed the universe's expansion in the local universe (or the late route, shown in the upper half of the graphic). The letters corresponding to each technique are plotted on the bridge on the right. The location of each dot on the bridge road represents the measured value of the H_0 , while the length of the associated bar shows the estimated amount of uncertainty in the measurements. The combined average from the seven methods from the late route yields a H_0 value of $73 \text{ km s}^{-1} \text{ Mpc}^{-1}$. This number is at odds with the combined value of the techniques used to calculate the universe's expansion rate from the early route. Their combined value for the H_0 is $67.4 \text{ km s}^{-1} \text{ Mpc}^{-1}$. Abridged version. Original graphic credit: NASA, ESA, and A. James (STScI).

International Symposium on the Physics of Ionized Gases, held between 05th - 09th September 2022, for allowing presenting our work as an invited contribution. We are grateful to Prof. Jian-Min Wang for providing his slim disk SED models and to Prof. Bożena Czerny for fruitful discussions.

DATA AVAILABILITY STATEMENT

All data incorporated in this work can be made available upon request to the authors.

REFERENCES

- Abramowicz, M. A., Czerny, B., Lasota, J. P., and Szuszkiewicz, E. (1988). Slim accretion disks. *The Astrophysical Journal* 332, 646–658. doi:10.1086/166683
- Ai, Y. L., Yuan, W., Zhou, H., Wang, T. G., Dong, X. B., Wang, J. G., et al. (2013). A Comparative Study of Optical/Ultraviolet Variability of Narrow-line Seyfert 1 and Broad-line Seyfert 1 Active Galactic Nuclei. *The Astronomical Journal* 145, 90. doi:10.1088/0004-6256/145/4/90
- Ai, Y. L., Yuan, W., Zhou, H. Y., Wang, T. G., and Zhang, S. H. (2011). X-ray Properties of Narrow-line Seyfert 1 Galaxies with Very Small Broadline Widths. *The Astrophysical Journal* 727, 31. doi:10.1088/0004-637X/727/1/31
- Antonucci, R. (1993). Unified models for active galactic nuclei and quasars. *Annual Review of Astronomy and Astrophysics* 31, 473–521. doi:10.1146/annurev.aa.31.090193.002353
- Antonucci, R. (2012). A panchromatic review of thermal and nonthermal active galactic nuclei. *Astronomical and Astrophysical Transactions* 27, 557–602
- Arnaud, K. A., Branduardi-Raymont, G., Culhane, J. L., Fabian, A. C., Hazard, C., McGlynn, T. A., et al. (1985). EXOSAT observations of a strong soft X-ray excess in MKN 841. *Monthly Notices of the Royal Astronomical Society* 217, 105–113. doi:10.1093/mnras/217.1.105
- Baldwin, J. A., Ferland, G. J., Korista, K. T., Hamann, F., and LaCluyzé, A. (2004). The Origin of Fe II Emission in Active Galactic Nuclei. *The Astrophysical Journal* 615, 610–624. doi:10.1086/424683
- Barth, A. J., Pancoast, A., Bennert, V. N., Brewer, B. J., Canalizo, G., Filippenko, A. V., et al. (2013). The Lick AGN Monitoring Project 2011: Fe II Reverberation from the Outer Broad-line Region. *The Astrophysical Journal* 769, 128. doi:10.1088/0004-637X/769/2/128
- Bensch, K., del Olmo, A., Sulentic, J., Perea, J., and Marziani, P. (2015). Measures of the Soft X-ray Excess as an Eigenvector 1 Parameter for Active Galactic Nuclei. *Journal of Astrophysics and Astronomy* 36, 467–474. doi:10.1007/s12036-015-9355-8
- Bentz, M. C., Cackett, E. M., Crenshaw, D. M., Horne, K., Street, R., and Ou-Yang, B. (2016). A Reverberation-based Black Hole Mass for MCG-06-30-15. *The Astrophysical Journal* 830, 136. doi:10.3847/0004-637X/830/2/136
- Bentz, M. C., Denney, K. D., Grier, C. J., Barth, A. J., Peterson, B. M., Vestergaard, M., et al. (2013). The Low-luminosity End of the Radius-Luminosity Relationship for Active Galactic Nuclei. *The Astrophysical Journal* 767, 149. doi:10.1088/0004-637X/767/2/149
- Bentz, M. C., Horenstein, D., Bazhaw, C., Manne-Nicholas, E. R., Ou-Yang, B. J., Anderson, M., et al. (2014). The Mass of the Central Black Hole in the Nearby Seyfert Galaxy NGC 5273. *The Astrophysical Journal* 796, 8. doi:10.1088/0004-637X/796/1/8
- Bentz, M. C., Peterson, B. M., Netzer, H., Pogge, R. W., and Vestergaard, M. (2009). The Radius-Luminosity Relationship for Active Galactic Nuclei: The Effect of Host-Galaxy Starlight on Luminosity Measurements. II. The Full Sample of Reverberation-Mapped AGNs. *The Astrophysical Journal* 697, 160–181. doi:10.1088/0004-637X/697/1/160

- Berton, M., Foschini, L., Caccianiga, A., Ciroi, S., Congiu, E., Cracco, V., et al. (2017). An orientation-based unification of young jetted active galactic nuclei: the case of 3C 286. *Frontiers in Astronomy and Space Sciences* 4, 8. doi:10.3389/fspas.2017.00008
- Blandford, R. D. and McKee, C. F. (1982). Reverberation mapping of the emission line regions of Seyfert galaxies and quasars. *The Astrophysical Journal* 255, 419–439. doi:10.1086/159843
- Boissay, R., Ricci, C., and Paltani, S. (2016). A hard X-ray view of the soft excess in AGN. *Astronomy and Astrophysics* 588, A70. doi:10.1051/0004-6361/201526982
- Boroson, T. A. (2002). Black Hole Mass and Eddington Ratio as Drivers for the Observable Properties of Radio-loud and Radio-quiet QSOs. *The Astrophysical Journal* 565, 78–85. doi:10.1086/324486
- Boroson, T. A. and Green, R. F. (1992). The Emission-Line Properties of Low-Redshift Quasi-stellar Objects. *The Astrophysical Journal Supplements* 80, 109. doi:10.1086/191661
- Buendia-Rios, T. M., Negrete, C. A., Marziani, P., and Dultzin, D. (2023). Statistical analysis of Al III and C III] emission lines as virial black hole mass estimators in quasars. *Astronomy & Astrophysics* 669, A135. doi:10.1051/0004-6361/202244177
- Caccianiga, A., Antón, S., Ballo, L., Foschini, L., Maccacaro, T., Della Ceca, R., et al. (2015). WISE colours and star formation in the host galaxies of radio-loud narrow-line Seyfert 1. *Monthly Notices of the Royal Astronomical Society* 451, 1795–1805. doi:10.1093/mnras/stv939
- Carniani, S., Marconi, A., Maiolino, R., Balmaverde, B., Brusa, M., Cano-Díaz, M., et al. (2015). Ionised outflows in $z \sim 2.4$ quasar host galaxies. *Astronomy and Astrophysics* 580, A102. doi:10.1051/0004-6361/201526557
- Cavaliere, A. and Vittorini, V. (2000). The Fall of the Quasar Population. *The Astrophysical Journal* 543, 599–610. doi:10.1086/317155
- Collier, S., Horne, K., Wanders, I., and Peterson, B. M. (1999). A new direct method for measuring the Hubble constant from reverberating accretion discs in active galaxies. *Monthly Notices of the Royal Astronomical Society* 302, L24–L28. doi:10.1046/j.1365-8711.1999.02250.x
- Collin, S., Kawaguchi, T., Peterson, B. M., and Vestergaard, M. (2006). Systematic effects in measurement of black hole masses by emission-line reverberation of active galactic nuclei: Eddington ratio and inclination. *Astronomy and Astrophysics* 456, 75–90. doi:10.1051/0004-6361:20064878
- Collin-Souffrin, S., Dyson, J. E., McDowell, J. C., and Perry, J. J. (1988). The environment of active galactic nuclei - I. A two-component broad emission line model. *Monthly Notices of the Royal Astronomical Society* 232, 539–550. doi:10.1093/mnras/232.3.539
- Collinson, J. S. (2016). *Spectral and temporal studies of supermassive black holes*. Ph.D. thesis, Durham University, UK
- Crummy, J., Fabian, A. C., Gallo, L., and Ross, R. R. (2006). An explanation for the soft X-ray excess in active galactic nuclei. *Monthly Notices of the Royal Astronomical Society* 365, 1067–1081. doi:10.1111/j.1365-2966.2005.09844.x
- Czerny, B. and Elvis, M. (1987). Constraints on quasar accretion disks from the optical/ultraviolet/soft X-ray big bump. *The Astrophysical Journal* 321, 305–320. doi:10.1086/165630
- Czerny, B., Hryniewicz, K., Maity, I., Schwarzenberg-Czerny, A., Życki, P. T., and Bilicki, M. (2013). Towards equation of state of dark energy from quasar monitoring: Reverberation strategy. *Astronomy and Astrophysics* 556, A97. doi:10.1051/0004-6361/201220832
- Czerny, B., Li, Y.-R., Hryniewicz, K., Panda, S., Wildy, C., Sniegowska, M., et al. (2017). Failed Radiatively Accelerated Dusty Outflow Model of the Broad Line Region in Active Galactic Nuclei. I. Analytical Solution. *The Astrophysical Journal* 846, 154. doi:10.3847/1538-4357/aa8810
- Czerny, B., Martínez-Aldama, M. L., Wojtkowska, G., Zajaček, M., Marziani, P., Dultzin, D., et al.

- (2021). Dark Energy Constraints from Quasar Observations. *Acta Physica Polonica A* 139, 389–393. doi:10.12693/APhysPolA.139.389
- Czerny, B., Olejak, A., Rałowski, M., Kozłowski, S., Martínez Aldama, M. L., Zajacek, M., et al. (2019). Time Delay Measurement of Mg II Line in CTS C30.10 with SALT. *The Astrophysical Journal* 880, 46. doi:10.3847/1538-4357/ab2913
- Davidson, K. (1977). On photoionization analyses of emission spectra of quasars. *The Astrophysical Journal* 218, 20–32. doi:10.1086/155653
- Davidson, K. and Netzer, H. (1979). The emission lines of quasars and similar objects. *Reviews of Modern Physics* 51, 715–766. doi:10.1103/RevModPhys.51.715
- Decarli, R., Dotti, M., and Treves, A. (2011). Geometry and inclination of the broad-line region in blazars. *Monthly Notices of the Royal Astronomical Society* 413, 39–46. doi:10.1111/j.1365-2966.2010.18102.x
- D’Onofrio, M., Marziani, P., and Chiosi, C. (2021). Past, Present and Future of the Scaling Relations of Galaxies and Active Galactic Nuclei. *Frontiers in Astronomy and Space Sciences* 8, 157. doi:10.3389/fspas.2021.694554
- Du, P., Hu, C., Lu, K.-X., Huang, Y.-K., Cheng, C., Qiu, J., et al. (2015). Supermassive Black Holes with High Accretion Rates in Active Galactic Nuclei. IV. $H\beta$ Time Lags and Implications for Super-Eddington Accretion. *The Astrophysical Journal* 806, 22. doi:10.1088/0004-637X/806/1/22
- Du, P., Hu, C., Lu, K.-X., Wang, F., Qiu, J., Li, Y.-R., et al. (2014). Supermassive Black Holes with High Accretion Rates in Active Galactic Nuclei. I. First Results from a New Reverberation Mapping Campaign. *The Astrophysical Journal* 782, 45. doi:10.1088/0004-637X/782/1/45
- Du, P., Lu, K.-X., Zhang, Z.-X., Huang, Y.-K., Wang, K., Hu, C., et al. (2016a). Supermassive Black Holes with High Accretion Rates in Active Galactic Nuclei. V. A New Size-Luminosity Scaling Relation for the Broad-line Region. *The Astrophysical Journal* 825, 126. doi:10.3847/0004-637X/825/2/126
- Du, P. and Wang, J.-M. (2019). The Radius-Luminosity Relationship Depends on Optical Spectra in Active Galactic Nuclei. *The Astrophysical Journal* 886, 42. doi:10.3847/1538-4357/ab4908
- Du, P., Wang, J.-M., Hu, C., Ho, L. C., Li, Y.-R., and Bai, J.-M. (2016b). The Fundamental Plane of the Broad-line Region in Active Galactic Nuclei. *The Astrophysical Journal Letters* 818, L14. doi:10.3847/2041-8205/818/1/L14
- Du, P., Zhang, Z.-X., Wang, K., Huang, Y.-K., Zhang, Y., Lu, K.-X., et al. (2018). Supermassive Black Holes with High Accretion Rates in Active Galactic Nuclei. IX. 10 New Observations of Reverberation Mapping and Shortened $H\beta$ Lags. *The Astrophysical Journal* 856, 6. doi:10.3847/1538-4357/aaae6b
- Dultzin, D., Marziani, P., de Diego, J. A., Negrete, C. A., Del Olmo, A., Martínez-Aldama, M. L., et al. (2020). Extreme quasars as distance indicators in cosmology. *Frontiers in Astronomy and Space Sciences* 6, 80. doi:10.3389/fspas.2019.00080
- Elvis, M. and Karovska, M. (2002). Quasar Parallax: A Method for Determining Direct Geometrical Distances to Quasars. *The Astrophysical Journal Letters* 581, L67–L70. doi:10.1086/346015
- Elvis, M., Wilkes, B. J., McDowell, J. C., Green, R. F., Bechtold, J., Willner, S. P., et al. (1994). Atlas of quasar energy distributions. *The Astrophysical Journal Supplements* 95, 1–68. doi:10.1086/192093
- Evans, C., Puech, M., Afonso, J., Almaini, O., Amram, P., Aussel, H., et al. (2015). The Science Case for Multi-Object Spectroscopy on the European ELT. *arXiv e-prints*, arXiv:1501.04726
- Faber, S. M. and Jackson, R. E. (1976). Velocity dispersions and mass-to-light ratios for elliptical galaxies. *The Astrophysical Journal* 204, 668–683. doi:10.1086/154215
- Fabian, A. C., Lohfink, A., Kara, E., Parker, M. L., Vasudevan, R., and Reynolds, C. S. (2015). Properties of AGN coronae in the NuSTAR era. *Monthly Notices of the Royal Astronomical Society* 451, 4375–4383. doi:10.1093/mnras/stv1218

- Fausnaugh, M. M., Grier, C. J., Bentz, M. C., Denney, K. D., De Rosa, G., Peterson, B. M., et al. (2017). Reverberation Mapping of Optical Emission Lines in Five Active Galaxies. *The Astrophysical Journal* 840, 97. doi:10.3847/1538-4357/aa6d52
- Ferland, G. J., Done, C., Jin, C., Landt, H., and Ward, M. J. (2020). State-of-the-art AGN SEDs for photoionization models: BLR predictions confront the observations. *Monthly Notices of the Royal Astronomical Society* 494, 5917–5922. doi:10.1093/mnras/staa1207
- Fraix-Burnet, D., Marziani, P., D’Onofrio, M., and Dultzin, D. (2017). The phylogeny of quasars and the ontogeny of their central black holes. *Frontiers in Astronomy and Space Sciences* 4, 1. doi:10.3389/fspas.2017.00001
- Ganci, V., Marziani, P., D’Onofrio, M., del Olmo, A., Bon, E., Bon, N., et al. (2019). Radio loudness along the quasar main sequence. *Astronomy and Astrophysics* 630, A110. doi:10.1051/0004-6361/201936270
- Gardner, J. P., Mather, J. C., Clampin, M., Doyon, R., Greenhouse, M. A., Hammel, H. B., et al. (2006). The James Webb Space Telescope. *Space Science Reviews* 123, 485–606. doi:10.1007/s11214-006-8315-7
- Garnica, K., Negrete, C. A., Marziani, P., Dultzin, D., Śniegowska, M., and Panda, S. (2022). High metal content of highly accreting quasars: Analysis of an extended sample. *Astronomy and Astrophysics* 667, A105. doi:10.1051/0004-6361/202142837
- Gaskell, C. M. (1982). A redshift difference between high and low ionization emission-line regions in QSO’s-evidence for radial motions. *The Astrophysical Journal* 263, 79–86. doi:10.1086/160481
- Giannuzzo, M. E., Mignoli, M., Stirpe, G. M., and Comastri, A. (1998). A search for variability in Narrow Line Seyfert 1 Galaxies. II. New data from the Loiano monitoring programme. *Astronomy and Astrophysics* 330, 894–900
- Giustini, M. and Proga, D. (2019). A global view of the inner accretion and ejection flow around super massive black holes. Radiation-driven accretion disk winds in a physical context. *Astronomy and Astrophysics* 630, A94. doi:10.1051/0004-6361/201833810
- Goodrich, R. W. (1989). Spectropolarimetry of “Narrow-Line” Seyfert 1 Galaxies. *The Astrophysical Journal* 342, 224. doi:10.1086/167586
- Greenstein, J. L. and Schmidt, M. (1964). The Quasi-Stellar Radio Sources 3C 48 and 3C 273. *The Astrophysical Journal* 140, 1. doi:10.1086/147889
- Grier, C. J., Trump, J. R., Shen, Y., Horne, K., Kinemuchi, K., McGreer, I. D., et al. (2017). The Sloan Digital Sky Survey Reverberation Mapping Project: $H\alpha$ and $H\beta$ Reverberation Measurements from First-year Spectroscopy and Photometry. *The Astrophysical Journal* 851, 21. doi:10.3847/1538-4357/aa98dc
- Grupe, D. (2004). A Complete Sample of Soft X-Ray-selected AGNs. II. Statistical Analysis. *The Astronomical Journal* 127, 1799–1810. doi:10.1086/382516
- Grupe, D., Komossa, S., Leighly, K. M., and Page, K. L. (2010). The Simultaneous Optical-to-X-Ray Spectral Energy Distribution of Soft X-Ray Selected Active Galactic Nuclei Observed by Swift. *The Astrophysical Journal Supplements* 187, 64–106. doi:10.1088/0067-0049/187/1/64
- Haas, M., Chini, R., Ramolla, M., Pozo Nuñez, F., Westhues, C., Watermann, R., et al. (2011). Photometric AGN reverberation mapping - an efficient tool for BLR sizes, black hole masses, and host-subtracted AGN luminosities. *Astronomy and Astrophysics* 535, A73. doi:10.1051/0004-6361/201117325
- Hamann, F. and Ferland, G. (1993). The Chemical Evolution of QSOs and the Implications for Cosmology and Galaxy Formation. *The Astrophysical Journal* 418, 11. doi:10.1086/173366
- Hamann, F. and Ferland, G. (1999). Elemental Abundances in Quasistellar Objects: Star Formation and Galactic Nuclear Evolution at High Redshifts. *Annual Review of Astronomy & Astrophysics* 37, 487–531. doi:10.1146/annurev.astro.37.1.487

- Harrison, C. (2014). *Observational constraints on the influence of active galactic nuclei on the evolution of galaxies*. Ph.D. thesis, Durham University
- Hopkins, P. F., Hernquist, L., Cox, T. J., Di Matteo, T., Robertson, B., and Springel, V. (2006). A Unified, Merger-driven Model of the Origin of Starbursts, Quasars, the Cosmic X-Ray Background, Supermassive Black Holes, and Galaxy Spheroids. *The Astrophysical Journal Supplements* 163, 1–49. doi:10.1086/499298
- Horne, K., Korista, K. T., and Goad, M. R. (2003). Quasar tomography: unification of echo mapping and photoionization models. *Monthly Notices of the Royal Astronomical Society* 339, 367–386. doi:10.1046/j.1365-8711.2003.06036.x
- Horne, K., Peterson, B. M., Collier, S. J., and Netzer, H. (2004). Observational Requirements for High-Fidelity Reverberation Mapping. *Publications of the Astronomical Society of the Pacific* 116, 465–476. doi:10.1086/420755
- Hu, C., Du, P., Lu, K.-X., Li, Y.-R., Wang, F., Qiu, J., et al. (2015). Supermassive Black Holes with High Accretion Rates in Active Galactic Nuclei. III. Detection of Fe II Reverberation in Nine Narrow-line Seyfert 1 Galaxies. *The Astrophysical Journal* 804, 138. doi:10.1088/0004-637X/804/2/138
- Jakobsen, P., Ferruit, P., Alves de Oliveira, C., Arribas, S., Bagnasco, G., Barho, R., et al. (2022). The Near-Infrared Spectrograph (NIRSpec) on the James Webb Space Telescope. I. Overview of the instrument and its capabilities. *Astronomy and Astrophysics* 661, A80. doi:10.1051/0004-6361/202142663
- Jin, C., Ward, M., and Done, C. (2012a). A combined optical and X-ray study of unobscured type 1 active galactic nuclei - II. Relation between X-ray emission and optical spectra. *Monthly Notices of the Royal Astronomical Society* 422, 3268–3284. doi:10.1111/j.1365-2966.2012.20847.x
- Jin, C., Ward, M., Done, C., and Gelbord, J. (2012b). A combined optical and X-ray study of unobscured type 1 active galactic nuclei - I. Optical spectra and spectral energy distribution modelling. *Monthly Notices of the Royal Astronomical Society* 420, 1825–1847. doi:10.1111/j.1365-2966.2011.19805.x
- Kamraj, N., Brightman, M., Harrison, F. A., Stern, D., García, J. A., Baloković, M., et al. (2022). X-Ray Coronal Properties of Swift/BAT-selected Seyfert 1 Active Galactic Nuclei. *The Astrophysical Journal* 927, 42. doi:10.3847/1538-4357/ac45f6
- Kaspi, S., Smith, P. S., Netzer, H., Maoz, D., Jannuzi, B. T., and Giveon, U. (2000). Reverberation Measurements for 17 Quasars and the Size-Mass-Luminosity Relations in Active Galactic Nuclei. *The Astrophysical Journal* 533, 631–649. doi:10.1086/308704
- Khadka, N., Martínez-Aldama, M. L., Zajaček, M., Czerny, B., and Ratra, B. (2022). Do reverberation-measured $H\beta$ quasars provide a useful test of cosmology? *Monthly Notices of the Royal Astronomical Society* 513, 1985–2005. doi:10.1093/mnras/stac914
- Khadka, N., Yu, Z., Zajaček, M., Martinez-Aldama, M. L., Czerny, B., and Ratra, B. (2021). Standardizing reverberation-measured Mg II time-lag quasars, by using the radius-luminosity relation, and constraining cosmological model parameters. *Monthly Notices of the Royal Astronomical Society* 508, 4722–4737. doi:10.1093/mnras/stab2807
- Kirkpatrick, A., Pope, A., Sajina, A., Roebuck, E., Yan, L., Armus, L., et al. (2015). The Role of Star Formation and an AGN in Dust Heating of $z = 0.3$ -2.8 Galaxies. I. Evolution with Redshift and Luminosity. *The Astrophysical Journal* 814, 9. doi:10.1088/0004-637X/814/1/9
- Kubota, A. and Done, C. (2018). A physical model of the broad-band continuum of AGN and its implications for the UV/X relation and optical variability. *Monthly Notices of the Royal Astronomical Society* 480, 1247–1262. doi:10.1093/mnras/sty1890
- Kwan, J. and Krolik, J. H. (1981). The formation of emission lines in quasars and Seyfert nuclei. *The Astrophysical Journal* 250, 478–507. doi:10.1086/159395

- Laor, A., Fiore, F., Elvis, M., Wilkes, B. J., and McDowell, J. C. (1997). The Soft X-Ray Properties of a Complete Sample of Optically Selected Quasars. II. Final Results. *The Astrophysical Journal* 477, 93–113. doi:10.1086/303696
- Laor, A. and Netzer, H. (1989). Massive thin accretion discs. - I. Calculated spectra. *Monthly Notices of the Royal Astronomical Society* 238, 897–916. doi:10.1093/mnras/238.3.897
- Laurenti, M., Piconcelli, E., Zappacosta, L., Tombesi, F., Vignali, C., Bianchi, S., et al. (2022). X-ray spectroscopic survey of highly accreting AGN. *Astronomy and Astrophysics* 657, A57. doi:10.1051/0004-6361/202141829
- Leighly, K. M. (1999). A Comprehensive Spectral and Variability Study of Narrow-Line Seyfert 1 Galaxies Observed by ASCA. II. Spectral Analysis and Correlations. *The Astrophysical Journal Supplements* 125, 317–348. doi:10.1086/313287
- Leighly, K. M. (2004). Hubble Space Telescope STIS Ultraviolet Spectral Evidence of Outflow in Extreme Narrow-Line Seyfert 1 Galaxies. II. Modeling and Interpretation. *The Astrophysical Journal* 611, 125–152. doi:10.1086/422089
- Leighly, K. M. and Moore, J. R. (2004). Hubble Space Telescope STIS Ultraviolet Spectral Evidence of Outflow in Extreme Narrow-Line Seyfert 1 Galaxies. I. Data and Analysis. *The Astrophysical Journal* 611, 107–124. doi:10.1086/422088
- Li, Y.-R., Songsheng, Y.-Y., Qiu, J., Hu, C., Du, P., Lu, K.-X., et al. (2018). Supermassive Black Holes with High Accretion Rates in Active Galactic Nuclei. VIII. Structure of the Broad-line Region and Mass of the Central Black Hole in Mrk 142. *The Astrophysical Journal* 869, 137. doi:10.3847/1538-4357/aaee6b
- Li, Y.-R., Wang, J.-M., and Bai, J.-M. (2016). A Non-parametric Approach to Constrain the Transfer Function in Reverberation Mapping. *The Astrophysical Journal* 831, 206. doi:10.3847/0004-637X/831/2/206
- Liu, H., Luo, B., Brandt, W. N., Brotherton, M. S., Gallagher, S. C., Ni, Q., et al. (2021). On the Observational Difference between the Accretion Disk-Corona Connections among Super- and Sub-Eddington Accreting Active Galactic Nuclei. *The Astrophysical Journal* 910, 103. doi:10.3847/1538-4357/abe37f
- Lu, K.-X., Du, P., Hu, C., Li, Y.-R., Zhang, Z.-X., Wang, K., et al. (2016). Reverberation Mapping of the Broad-line Region in NGC 5548: Evidence for Radiation Pressure? *The Astrophysical Journal* 827, 118. doi:10.3847/0004-637X/827/2/118
- Lubiński, P., Beckmann, V., Gibaud, L., Paltani, S., Papadakis, I. E., Ricci, C., et al. (2016). A comprehensive analysis of the hard X-ray spectra of bright Seyfert galaxies. *Monthly Notices of the Royal Astronomical Society* 458, 2454–2475. doi:10.1093/mnras/stw454
- Malkan, M. A. (1983). The ultraviolet excess of luminous quasars. II. Evidence for massive accretion disks. *The Astrophysical Journal* 268, 582–590. doi:10.1086/160981
- Malkan, M. A. and Sargent, W. L. W. (1982). The ultraviolet excess of Seyfert 1 galaxies and quasars. *The Astrophysical Journal* 254, 22–37. doi:10.1086/159701
- Marin, F. (2014). A compendium of AGN inclinations with corresponding UV/optical continuum polarization measurements. *Monthly Notices of the Royal Astronomical Society* 441, 551–564. doi:10.1093/mnras/stu593
- Marinello, M., Rodríguez-Ardila, A., Garcia-Rissmann, A., Sigut, T. A. A., and Pradhan, A. K. (2016). The Fe II Emission in Active Galactic Nuclei: Excitation Mechanisms and Location of the Emitting Region. *The Astrophysical Journal* 820, 116. doi:10.3847/0004-637X/820/2/116
- Marshall, J., Bolton, A., Bullock, J., Burgasser, A., Chambers, K., DePoy, D., et al. (2019). The Maunakea Spectroscopic Explorer. In *Bulletin of the American Astronomical Society*. vol. 51, 126

- Martínez-Aldama, M. L., Czerny, B., Kawka, D., Karas, V., Panda, S., Zajaček, M., et al. (2019). Can Reverberation-measured Quasars Be Used for Cosmology? *The Astrophysical Journal* 883, 170. doi:10.3847/1538-4357/ab3728
- Martínez-Aldama, M. L., Dultzin, D., Marziani, P., Sulentic, J. W., Bressan, A., Chen, Y., et al. (2015). O I and Ca II Observations in Intermediate Redshift Quasars. *The Astrophysical Journal Supplements* 217, 3. doi:10.1088/0067-0049/217/1/3
- Martínez-Aldama, M. L., Panda, S., Czerny, B., Marinello, M., Marziani, P., and Dultzin, D. (2021). The CaFe Project: Optical Fe II and Near-infrared Ca II Triplet Emission in Active Galaxies. II. The Driver(s) of the Ca II and Fe II and Its Potential Use as a Chemical Clock. *The Astrophysical Journal* 918, 29. doi:10.3847/1538-4357/ac03b6
- Marziani, P., del Olmo, A., D’Onofrio, M., Dultzin, D., Negrete, C. A., Martínez-Aldama, M. L., et al. (2018a). Narrow-line Seyfert 1s: what is wrong in a name? In *Revisiting Narrow-Line Seyfert 1 Galaxies and their Place in the Universe*. 2. doi:10.22323/1.328.0002
- Marziani, P., del Olmo, A., Martínez-Carballo, M. A., Martínez-Aldama, M. L., Stirpe, G. M., Negrete, C. A., et al. (2019). Black hole mass estimates in quasars. A comparative analysis of high- and low-ionization lines. *Astronomy and Astrophysics* 627, A88. doi:10.1051/0004-6361/201935265
- Marziani, P., Dultzin, D., del Olmo, A., D’Onofrio, M., de Diego, J. A., Stirpe, G. M., et al. (2021a). The quasar main sequence and its potential for cosmology. In *Nuclear Activity in Galaxies Across Cosmic Time*, eds. M. Pović, P. Marziani, J. Masegosa, H. Netzer, S. H. Negu, and S. B. Tessema. vol. 356, 66–71. doi:10.1017/S1743921320002598
- Marziani, P., Dultzin, D., Sulentic, J. W., Del Olmo, A., Negrete, C. A., Martínez-Aldama, M. L., et al. (2018b). A main sequence for quasars. *Frontiers in Astronomy and Space Sciences* 5, 6. doi:10.3389/fspas.2018.00006
- Marziani, P., Dultzin-Hacyan, D., and Sulentic, J. W. (2006). Accretion onto Supermassive Black Holes in Quasars: Learning from Optical/UV Observations. In *New Developments in Black Hole Research*, ed. P. V. Kreitler (Nova Press, New York). 123
- Marziani, P., Martínez Carballo, M. A., Sulentic, J. W., Del Olmo, A., Stirpe, G. M., and Dultzin, D. (2016). The most powerful quasar outflows as revealed by the Civ $\lambda 1549$ resonance line. *Astrophysics and Space Sciences* 361, 29. doi:10.1007/s10509-015-2611-1
- Marziani, P., Olmo, A. d., Negrete, C. A., Dultzin, D., Piconcelli, E., Vietri, G., et al. (2022). The Intermediate-ionization Lines as Virial Broadening Estimators for Population A Quasars. *The Astrophysical Journal Supplements* 261, 30. doi:10.3847/1538-4365/ac6fd6
- Marziani, P., Sniegowska, M., Panda, S., Czerny, B., Negrete, C. A., Dultzin, D., et al. (2021b). The Main Sequence View of Quasars Accreting at High Rates: Influence of Star Formation. *Research Notes of the American Astronomical Society* 5, 25. doi:10.3847/2515-5172/abe46a
- Marziani, P. and Sulentic, J. W. (2012). Estimating black hole masses in quasars using broad optical and UV emission lines. *NARev* 56, 49–63. doi:10.1016/j.newar.2011.09.001
- Marziani, P. and Sulentic, J. W. (2014a). Highly accreting quasars: sample definition and possible cosmological implications. *Monthly Notices of the Royal Astronomical Society* 442, 1211–1229. doi:10.1093/mnras/stu951
- Marziani, P. and Sulentic, J. W. (2014b). Quasars and their emission lines as cosmological probes. *Advances in Space Research* 54, 1331–1340. doi:10.1016/j.asr.2013.10.007
- Marziani, P., Sulentic, J. W., Negrete, C. A., Dultzin, D., Zamfir, S., and Bachev, R. (2010). Broad-line region physical conditions along the quasar eigenvector 1 sequence. *Monthly Notices of the Royal Astronomical Society* 409, 1033–1048. doi:10.1111/j.1365-2966.2010.17357.x

- Marziani, P., Sulentic, J. W., Plauchu-Frayn, I., and del Olmo, A. (2013). Low-Ionization Outflows in High Eddington Ratio Quasars. *The Astrophysical Journal* 764
- Marziani, P., Sulentic, J. W., Zwitter, T., Dultzin-Hacyan, D., and Calvani, M. (2001). Searching for the Physical Drivers of the Eigenvector 1 Correlation Space. *ApJ* 558, 553–560. doi:10.1086/322286
- Mathews, W. G. and Ferland, G. J. (1987). What heats the hot phase in active nuclei? *The Astrophysical Journal* 323, 456–467. doi:10.1086/165843
- Mathur, S. (2000). Narrow-line Seyfert 1 galaxies and the evolution of galaxies and active galaxies. *Monthly Notices of the Royal Astronomical Society* 314, L17–L20. doi:10.1046/j.1365-8711.2000.03530.x
- Matsuoka, Y., Kawara, K., and Oyabu, S. (2008). Low-Ionization Emission Regions in Quasars: Gas Properties Probed with Broad O I and Ca II Lines. *The Astrophysical Journal* 673, 62–68. doi:10.1086/524193
- McHardy, I. M., Koeding, E., Knigge, C., Uttley, P., and Fender, R. P. (2006). Active galactic nuclei as scaled-up Galactic black holes. *Nature* 444, 730–732. doi:10.1038/nature05389
- McLure, R. J. and Jarvis, M. J. (2002). Measuring the black hole masses of high-redshift quasars. *Monthly Notices of the Royal Astronomical Society* 337, 109–116. doi:10.1046/j.1365-8711.2002.05871.x
- Mineshige, S., Kawaguchi, T., Takeuchi, M., and Hayashida, K. (2000). Slim-Disk Model for Soft X-Ray Excess and Variability of Narrow-Line Seyfert 1 Galaxies. *Publications of the Astronomical Society of Japan* 52, 499–508
- Molina, M., Malizia, A., Bassani, L., Ursini, F., Bazzano, A., and Ubertini, P. (2019). Swift/XRT-NuSTAR spectra of type 1 AGN: confirming INTEGRAL results on the high-energy cut-off. *Monthly Notices of the Royal Astronomical Society* 484, 2735–2746. doi:10.1093/mnras/stz156
- Negrete, A., Dultzin, D., Marziani, P., and Sulentic, J. (2012). BLR Physical Conditions in Extreme Population A Quasars: a Method to Estimate Central Black Hole Mass at High Redshift. *The Astrophysical Journal* 757, 62
- Negrete, C. A., Dultzin, D., Marziani, P., Esparza, D., Sulentic, J. W., del Olmo, A., et al. (2018). Highly accreting quasars: The SDSS low-redshift catalog. *Astronomy and Astrophysics* 620, A118. doi:10.1051/0004-6361/201833285
- Negrete, C. A., Dultzin, D., Marziani, P., and Sulentic, J. W. (2014). A photoionization method for estimating BLR “size” in quasars. *Advances in Space Research* 54, 1355–1361. doi:10.1016/j.asr.2013.11.037
- Netzer, H. (2015). Revisiting the Unified Model of Active Galactic Nuclei. *Annual Review of Astronomy and Astrophysics* 53, 365–408. doi:10.1146/annurev-astro-082214-122302
- Netzer, H. (2019). Bolometric correction factors for active galactic nuclei. *Monthly Notices of the Royal Astronomical Society* 488, 5185–5191. doi:10.1093/mnras/stz2016
- Ojha, V., Chand, H., Dewangan, G. C., and Rakshit, S. (2020). A Comparison of X-Ray Photon Indices among the Narrow- and Broad-line Seyfert 1 Galaxies. *The Astrophysical Journal* 896, 95. doi:10.3847/1538-4357/ab94ac
- Osterbrock, D. E. and Ferland, G. J. (2006). *Astrophysics of gaseous nebulae and active galactic nuclei*
- Osterbrock, D. E. and Pogge, R. W. (1985). The spectra of narrow-line Seyfert 1 galaxies. *The Astrophysical Journal* 297, 166–176. doi:10.1086/163513
- Padovani, P., Alexander, D. M., Assef, R. J., De Marco, B., Giommi, P., Hickox, R. C., et al. (2017). Active galactic nuclei: what’s in a name? *Astronomy and Astrophysics Reviews* 25, 2. doi:10.1007/s00159-017-0102-9
- Padovani, P. and Rafanelli, P. (1988). Mass-luminosity relationships and accretion rates for Seyfert 1 galaxies and quasars. *Astronomy and Astrophysics* 205, 53–70

- Panagiotou, C. and Walter, R. (2020). NuSTAR view of Swift/BAT AGN: The R- Γ correlation. *Astronomy and Astrophysics* 640, A31. doi:10.1051/0004-6361/201937390
- Pancoast, A., Brewer, B. J., Treu, T., Park, D., Barth, A. J., Bentz, M. C., et al. (2014). Modelling reverberation mapping data - II. Dynamical modelling of the Lick AGN Monitoring Project 2008 data set. *Monthly Notices of the Royal Astronomical Society* 445, 3073–3091. doi:10.1093/mnras/stu1419
- Panda, S. (2021a). *Physical Conditions in the Broad-line Regions of Active Galaxies*. Ph.D. thesis, Polish Academy of Sciences, Institute of Physics
- Panda, S. (2021b). The CaFe project: Optical Fe II and near-infrared Ca II triplet emission in active galaxies: simulated EWs and the co-dependence of cloud size and metal content. *Astronomy and Astrophysics* 650, A154. doi:10.1051/0004-6361/202140393
- Panda, S. (2022). Parameterizing the AGN Radius–Luminosity Relation from the Eigenvector 1 Viewpoint. *Frontiers in Astronomy and Space Sciences* 9, 850409. doi:10.3389/fspas.2022.850409
- Panda, S., Czerny, B., Adhikari, T. P., Hryniewicz, K., Wildy, C., Kuraszkiewicz, J., et al. (2018). Modeling of the Quasar Main Sequence in the Optical Plane. *The Astrophysical Journal* 866, 115. doi:10.3847/1538-4357/aae209
- Panda, S., Czerny, B., Done, C., and Kubota, A. (2019a). CLOUDY View of the Warm Corona. *The Astrophysical Journal* 875, 133. doi:10.3847/1538-4357/ab11cb
- Panda, S., Czerny, B., and Wildy, C. (2017). The physical driver of the optical Eigenvector 1 in Quasar Main Sequence. *Frontiers in Astronomy and Space Sciences* 4, 33. doi:10.3389/fspas.2017.00033
- Panda, S., Martínez-Aldama, M. L., and Zajaček, M. (2019b). Current and future applications of Reverberation-mapped quasars in Cosmology. *Frontiers in Astronomy and Space Sciences* 6, 75. doi:10.3389/fspas.2019.00075
- Panda, S., Marziani, P., and Czerny, B. (2019c). The Quasar Main Sequence Explained by the Combination of Eddington Ratio, Metallicity, and Orientation. *The Astrophysical Journal* 882, 79. doi:10.3847/1538-4357/ab3292
- Pei, L., Barth, A. J., Aldering, G. S., Briley, M. M., Carroll, C. J., Carson, D. J., et al. (2014). Reverberation Mapping of the KEPLER Field AGN KA1858+4850. *The Astrophysical Journal* 795, 38. doi:10.1088/0004-637X/795/1/38
- Peterson, B. M. (1988). Emission-Line Variability in Seyfert Galaxies. *Publications of the Astronomical Society of the Pacific* 100, 18. doi:10.1086/132130
- Peterson, B. M. (1993). Reverberation Mapping of Active Galactic Nuclei. *Publications of the Astronomical Society of the Pacific* 105, 247. doi:10.1086/133140
- Peterson, B. M., Ferrarese, L., Gilbert, K. M., Kaspi, S., Malkan, M. A., Maoz, D., et al. (2004a). Central Masses and Broad-Line Region Sizes of Active Galactic Nuclei. II. A Homogeneous Analysis of a Large Reverberation-Mapping Database. *The Astrophysical Journal* 613, 682–699. doi:10.1086/423269
- Peterson, B. M., Ferrarese, L., Gilbert, K. M., Kaspi, S., Malkan, M. A., Maoz, D., et al. (2004b). Central Masses and Broad-Line Region Sizes of Active Galactic Nuclei. II. A Homogeneous Analysis of a Large Reverberation-Mapping Database. *The Astrophysical Journal* 613, 682–699. doi:10.1086/423269
- Petrucchi, P. O., Gronkiewicz, D., Rozanska, A., Belmont, R., Bianchi, S., Czerny, B., et al. (2020). Radiation spectra of warm and optically thick coronae in AGNs. *Astronomy and Astrophysics* 634, A85. doi:10.1051/0004-6361/201937011
- Phillips, M. M. (1978). Permitted Fe II Emission in Seyfert 1 Galaxies and QSOs I. Observations. *The Astrophysical Journal Supplements* 38, 187. doi:10.1086/190553
- Rakshit, S., Stalin, C. S., and Kotilainen, J. (2020). Spectral Properties of Quasars from Sloan Digital Sky Survey Data Release 14: The Catalog. *The Astrophysical Journal Supplements* 249, 17. doi:10.3847/

- 1538-4365/ab99c5
- Ricci, C., Ho, L. C., Fabian, A. C., Trakhtenbrot, B., Koss, M. J., Ueda, Y., et al. (2018). BAT AGN Spectroscopic Survey - XII. The relation between coronal properties of active galactic nuclei and the Eddington ratio. *Monthly Notices of the Royal Astronomical Society* 480, 1819–1830. doi:10.1093/mnras/sty1879
- Richards, G. T., Lacy, M., Storrie-Lombardi, L. J., Hall, P. B., Gallagher, S. C., Hines, D. C., et al. (2006). Spectral Energy Distributions and Multiwavelength Selection of Type 1 Quasars. *The Astrophysical Journal Supplements* 166, 470–497. doi:10.1086/506525
- Ross, R. R. and Fabian, A. C. (2005). A comprehensive range of X-ray ionized-reflection models. *Monthly Notices of the Royal Astronomical Society* 358, 211–216. doi:10.1111/j.1365-2966.2005.08797.x
- Runnoe, J. C., Brotherton, M. S., Shang, Z., Wills, B. J., and DiPompeo, M. A. (2013). The orientation dependence of quasar single-epoch black hole mass scaling relationships. *Monthly Notices of the Royal Astronomical Society* 429, 135–149. doi:10.1093/mnras/sts322
- Sadowski, A. (2011). Slim accretion disks around black holes. *arXiv e-prints*, arXiv:1108.0396
- Schmidt, M. (1963). 3C 273 : A Star-Like Object with Large Red-Shift. *Nature* 197, 1040. doi:10.1038/1971040a0
- Schmidt, M. and Green, R. F. (1983). Quasar evolution derived from the Palomar bright quasar survey and other complete quasar surveys. *The Astrophysical Journal* 269, 352–374. doi:10.1086/161048
- Shakura, N. I. and Sunyaev, R. A. (1973). Black holes in binary systems. Observational appearance. *Astronomy and Astrophysics* 24, 337–355
- Shen, Y. (2013). The mass of quasars. *Bulletin of the Astronomical Society of India* 41, 61–115
- Shen, Y., Hall, P. B., Horne, K., Zhu, G., McGreer, I., Simm, T., et al. (2019). The Sloan Digital Sky Survey Reverberation Mapping Project: Sample Characterization. *The Astrophysical Journal Supplements* 241, 34. doi:10.3847/1538-4365/ab074f
- Shen, Y. and Ho, L. C. (2014). The diversity of quasars unified by accretion and orientation. *Nature* 513, 210–213. doi:10.1038/nature13712
- Shen, Y., Richards, G. T., Strauss, M. A., Hall, P. B., Schneider, D. P., Snedden, S., et al. (2011). A Catalog of Quasar Properties from Sloan Digital Sky Survey Data Release 7. *The Astrophysical Journal Supplements* 194, 45. doi:10.1088/0067-0049/194/2/45
- Shields, G. A. (1978). Thermal continuum from accretion disks in quasars. *Nature* 272, 706–708. doi:10.1038/272706a0
- Sigut, T. A. A. and Pradhan, A. K. (2003). Predicted Fe II Emission-Line Strengths from Active Galactic Nuclei. *The Astrophysical Journal Supplements* 145, 15–37. doi:10.1086/345498
- Sigut, T. A. A., Pradhan, A. K., and Nahar, S. N. (2004). Theoretical Fe I-III Emission-Line Strengths from Active Galactic Nuclei with Broad-Line Regions. *The Astrophysical Journal* 611, 81–92. doi:10.1086/422027
- Śniegowska, M., Marziani, P., Czerny, B., Panda, S., Martínez-Aldama, M. L., del Olmo, A., et al. (2021). High Metal Content of Highly Accreting Quasars. *The Astrophysical Journal* 910, 115. doi:10.3847/1538-4357/abe1c8
- Spergel, D., Gehrels, N., Breckinridge, J., Donahue, M., Dressler, A., Gaudi, B. S., et al. (2013). Wide-Field InfraRed Survey Telescope-Astrophysics Focused Telescope Assets WFIRST-AFTA Final Report. *arXiv e-prints*, arXiv:1305.5422
- Sulentic, J. and Marziani, P. (2015). Quasars in the 4D Eigenvector 1 Context: a stroll down memory lane. *Frontiers in Astronomy and Space Sciences* 2, 6. doi:10.3389/fspas.2015.00006
- Sulentic, J. W., Bachev, R., Marziani, P., Negrete, C. A., and Dultzin, D. (2007). C IV λ 1549 as

- an Eigenvector 1 Parameter for Active Galactic Nuclei. *The Astrophysical Journal* 666, 757–777. doi:10.1086/519916
- Sulentic, J. W., Marziani, P., del Olmo, A., Dultzin, D., Perea, J., and Alenka Negrete, C. (2014). GTC spectra of $z \approx 2.3$ quasars: comparison with local luminosity analogs. *Astronomy and Astrophysics* 570, A96. doi:10.1051/0004-6361/201423975
- Sulentic, J. W., Marziani, P., and Dultzin-Hacyan, D. (2000a). Phenomenology of Broad Emission Lines in Active Galactic Nuclei. *Annual Review of Astronomy and Astrophysics* 38, 521–571. doi:10.1146/annurev.astro.38.1.521
- Sulentic, J. W., Zamfir, S., Marziani, P., and Dultzin, D. (2008). Our Search for an H-R Diagram of Quasars. In *Revista Mexicana de Astronomia y Astrofisica Conference Series*. vol. 32 of *Revista Mexicana de Astronomia y Astrofisica Conference Series*, 51–58
- Sulentic, J. W., Zwitter, T., Marziani, P., and Dultzin-Hacyan, D. (2000b). Eigenvector 1: An Optimal Correlation Space for Active Galactic Nuclei. *The Astrophysical Journal Letters* 536, L5–L9. doi:10.1086/312717
- Sun, J. and Shen, Y. (2015). Dissecting the Quasar Main Sequence: Insight from Host Galaxy Properties. *The Astrophysical Journal Letters* 804, L15. doi:10.1088/2041-8205/804/1/L15
- Takeuchi, S., Ohsuga, K., and Mineshige, S. (2013). Clumpy Outflows from Supercritical Accretion Flow. *Publications of the Astronomical Society of Japan* 65, 88. doi:10.1093/pasj/65.4.88
- Tortosa, A., Bianchi, S., Marinucci, A., Matt, G., and Petrucci, P. O. (2018). A NuSTAR census of coronal parameters in Seyfert galaxies. *Astronomy & Astrophysics* 614, A37. doi:10.1051/0004-6361/201732382
- Trakhtenbrot, B., Ricci, C., Koss, M. J., Schawinski, K., Mushotzky, R., Ueda, Y., et al. (2017). BAT AGN Spectroscopic Survey (BASS) - VI. The Γ_X - L/L_{Edd} relation. *Monthly Notices of the Royal Astronomical Society* 470, 800–814. doi:10.1093/mnras/stx1117
- Ulrich, M.-H., Maraschi, L., and Urry, C. M. (1997). Variability of Active Galactic Nuclei. *Annual Review of Astronomy and Astrophysics* 35, 445–502. doi:10.1146/annurev.astro.35.1.445
- Urry, C. M. and Padovani, P. (1995). Unified Schemes for Radio-Loud Active Galactic Nuclei. *Publications of the Astronomical Society of the Pacific* 107, 803. doi:10.1086/133630
- Verner, E. M., Verner, D. A., Korista, K. T., Ferguson, J. W., Hamann, F., and Ferland, G. J. (1999). Numerical Simulations of Fe II Emission Spectra. *The Astrophysical Journal Supplements* 120, 101–112. doi:10.1086/313171
- Vestergaard, M. and Peterson, B. M. (2006). Determining Central Black Hole Masses in Distant Active Galaxies and Quasars. II. Improved Optical and UV Scaling Relationships. *The Astrophysical Journal* 641, 689–709. doi:10.1086/500572
- Vietri, G., Piconcelli, E., Bischetti, M., Duras, F., Martocchia, S., Bongiorno, A., et al. (2018). The WISSH quasars project. IV. Broad line region versus kiloparsec-scale winds. *Astronomy and Astrophysics* 617, A81. doi:10.1051/0004-6361/201732335
- Walter, R. and Fink, H. H. (1993). The ultraviolet to soft X-ray bump of Seyfert 1 type active galactic nuclei. *Astronomy and Astrophysics* 274, 105
- Wandel, A., Peterson, B. M., and Malkan, M. A. (1999). Central Masses and Broad-Line Region Sizes of Active Galactic Nuclei. I. Comparing the Photoionization and Reverberation Techniques. *The Astrophysical Journal* 526, 579–591. doi:10.1086/308017
- Wang, A., An, T., Cheng, X., Ho, L. C., Kellermann, K. I., Baan, W. A., et al. (2022). VLBI observations of a sample of palomar-green quasars I: parsec-scale morphology. *Monthly Notices of the Royal Astronomical Society* doi:10.1093/mnras/stac3091
- Wang, J.-M., Du, P., Hu, C., Netzer, H., Bai, J.-M., Lu, K.-X., et al. (2014a). Supermassive Black Holes

- with High Accretion Rates in Active Galactic Nuclei. II. The Most Luminous Standard Candles in the Universe. *The Astrophysical Journal* 793, 108. doi:10.1088/0004-637X/793/2/108
- Wang, J.-M., Du, P., Li, Y.-R., Ho, L. C., Hu, C., and Bai, J.-M. (2014b). A New Approach to Constrain Black Hole Spins in Active Galaxies Using Optical Reverberation Mapping. *The Astrophysical Journal Letters* 792, L13. doi:10.1088/2041-8205/792/1/L13
- Wang, J.-M., Du, P., Valls-Gabaud, D., Hu, C., and Netzer, H. (2013). Super-Eddington Accreting Massive Black Holes as Long-Lived Cosmological Standards. *Physical Review Letters* 110, 081301. doi:10.1103/PhysRevLett.110.081301
- Wang, J.-M., Qiu, J., Du, P., and Ho, L. C. (2014c). Self-shadowing Effects of Slim Accretion Disks in Active Galactic Nuclei: The Diverse Appearance of the Broad-line Region. *The Astrophysical Journal* 797, 65. doi:10.1088/0004-637X/797/1/65
- Watarai, K.-Y., Fukue, J., Takeuchi, M., and Mineshige, S. (2000). Galactic Black-Hole Candidates Shining at the Eddington Luminosity. *Publications of the Astronomical Society of Japan* 52, 133
- Watson, D., Denney, K. D., Vestergaard, M., and Davis, T. M. (2011). A New Cosmological Distance Measure Using Active Galactic Nuclei. *The Astrophysical Journal Letters* 740, L49. doi:10.1088/2041-8205/740/2/L49
- Weedman, D. W. (1976). Luminosities of Seyfert galaxies and QSOs. *The Astrophysical Journal* 208, 30–36. doi:10.1086/154577
- Weedman, D. W. (1977). Seyfert galaxies. *Annual Review of Astronomy and Astrophysics* 15, 69–95. doi:10.1146/annurev.aa.15.090177.000441
- Wills, B. J., Netzer, H., and Wills, D. (1985). Broad emission features in QSOs and active galactic nuclei. II - New observations and theory of Fe II and H I emission. *The Astrophysical Journal* 288, 94–116. doi:10.1086/162767
- Yang, G., Boquien, M., Brandt, W. N., Buat, V., Burgarella, D., Ciesla, L., et al. (2022). Fitting AGN/Galaxy X-Ray-to-radio SEDs with CIGALE and Improvement of the Code. *The Astrophysical Journal* 927, 192. doi:10.3847/1538-4357/ac4971
- Zajaček, M., Czerny, B., Martinez-Aldama, M. L., Rałowski, M., Olejak, A., Przyłuski, R., et al. (2021). Time Delay of Mg II Emission Response for the Luminous Quasar HE 0435-4312: toward Application of the High-accretor Radius-Luminosity Relation in Cosmology. *The Astrophysical Journal* 912, 10. doi:10.3847/1538-4357/abe9b2
- Zappacosta, L., Piconcelli, E., Giustini, M., Vietri, G., Duras, F., Miniutti, G., et al. (2020). The WISSH quasars project. VII. The impact of extreme radiative field in the accretion disc and X-ray corona interplay. *Astronomy and Astrophysics* 635, L5. doi:10.1051/0004-6361/201937292
- Zdziarski, A. A., Ghisellini, G., George, I. M., Svensson, R., Fabian, A. C., and Done, C. (1990). Electron-Positron Pairs, Compton Reflection, and the X-Ray Spectra of Active Galactic Nuclei. *The Astrophysical Journal Letters* 363, L1. doi:10.1086/185851
- Zhang, Z.-X., Du, P., Smith, P. S., Zhao, Y., Hu, C., Xiao, M., et al. (2019). Kinematics of the Broad-line Region of 3C 273 from a 10 yr Reverberation Mapping Campaign. *The Astrophysical Journal* 876, 49. doi:10.3847/1538-4357/ab1099